



Behaviour and design of high strength steel homogeneous and hybrid welded I-section beams

Yufei Zhu^a, Xiang Yun^{b,*}, Leroy Gardner^a

^a Department of Civil and Environmental Engineering, Imperial College London, London SW7 2AZ, UK

^b Department of Civil and Structural Engineering, The University of Sheffield, Sheffield S1 3JD, UK

ARTICLE INFO

Keywords:

Bending tests
Cross-section classification
Finite element modelling
High strength steel (HSS)
Hybrid section
Rotation capacity
Welded I-section

ABSTRACT

The behaviour and design of high strength steel (HSS) beams are addressed in the present study. Six in-plane three-point bending tests on three different welded I-sections – two homogeneous S690 steel welded I-sections and one hybrid welded I-section with S690 steel flanges and an S355 steel web, were first conducted. The beam tests were carried out in major axis bending and a bespoke restraint system was designed and employed in the test programme to prevent lateral-torsional buckling. Following the experimental investigation, a thorough finite element (FE) modelling programme was performed, which included a validation study confirming the accuracy of the developed FE models in replicating the flexural behaviour of HSS welded I-section beams, and a parametric study generating additional FE data on HSS welded I-section beams over a broader range of cross-sectional slendernesses, steel grades and loading configurations. The test results obtained in the present study and collected from the literature, together with the generated FE data from the parametric study, were used to evaluate the suitability of the current Eurocode 3 cross-section slenderness limits for HSS homogeneous and hybrid welded I-sections in bending. It is shown that the current Eurocode Class 2 and Class 3 slenderness limits are suitable for the classification of the outstand flange (in compression) and internal web (in bending) elements of both HSS homogeneous and hybrid welded I-sections subjected to major axis bending, while stricter Class 1 slenderness limits are considered necessary to achieve sufficient rotation capacity for plastic design. The findings from the present study indicate that plastic design can be used for HSS structures, provided the proposed stricter Class 1 slenderness limits are employed.

1. Introduction

In recent decades, high strength steels (HSS), generally defined as those with nominal yield strengths greater than or equal to 460 MPa, are gaining increasing use in the structural engineering industry [1–3], particularly for heavily loaded structural components in long-span bridges, high-rise buildings and stadia. Compared with normal strength steels (NSS), the use of HSS enables the selection of smaller cross-section sizes for structural components, resulting in reductions in weight, as well as enabling more streamlined and elegant structures. In addition to material savings, a lighter structure generally requires smaller foundations and reduced transportation and construction times and costs, thereby contributing to lower CO₂ emissions and energy use.

HSS I-sections are generally fabricated by welding together two flange plates and a web plate, enabling the use of different steel grades for the flanges and the web. For structural members that resist primarily

bending moment, hybrid HSS welded I-sections, in which the flange plates are made of a higher strength steel than the web, are often more cost-effective than their homogenous HSS counterparts since the web of a cross-section only contributes a modest amount to the total bending resistance; hence, it can be more economical to use a less expensive lower strength steel in the web than in the flanges. While there is a strong body of research on homogeneous HSS welded I-section [4–10] columns, a relatively limited number of studies have been performed on the flexural behaviour of HSS homogeneous and hybrid welded I-section beams. McDermott [11] tested a total of nine A514 steel (i.e. with a nominal yield strength of 690 MPa) I-shaped beams subjected to either pure bending or bending with moment gradient, and highlighted the potential use of plastic design for HSS structures. Beg and Hladnik [12] studied the local stability of welded I-section beams made of HSS with a yield strength around 800 MPa, and proposed an analytical expression to determine the Class 3 slenderness limit for HSS welded I-sections in

* Corresponding author.

E-mail address: x.yun@sheffield.ac.uk (X. Yun).

<https://doi.org/10.1016/j.engstruct.2022.115275>

Received 28 May 2022; Received in revised form 31 October 2022; Accepted 6 November 2022

Available online 24 November 2022

0141-0296/© 2022 The Author(s). Published by Elsevier Ltd. This is an open access article under the CC BY-NC-ND license (<http://creativecommons.org/licenses/by-nc-nd/4.0/>).

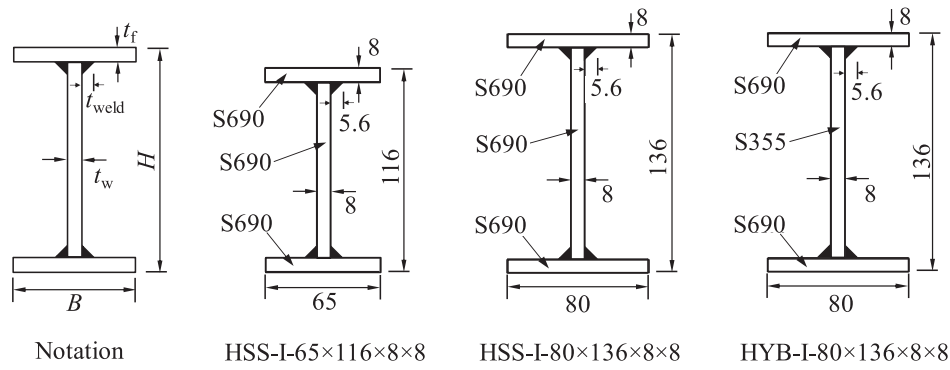


Fig. 1. Notation and nominal dimensions of the three investigated welded I-sections (dimensions in mm).

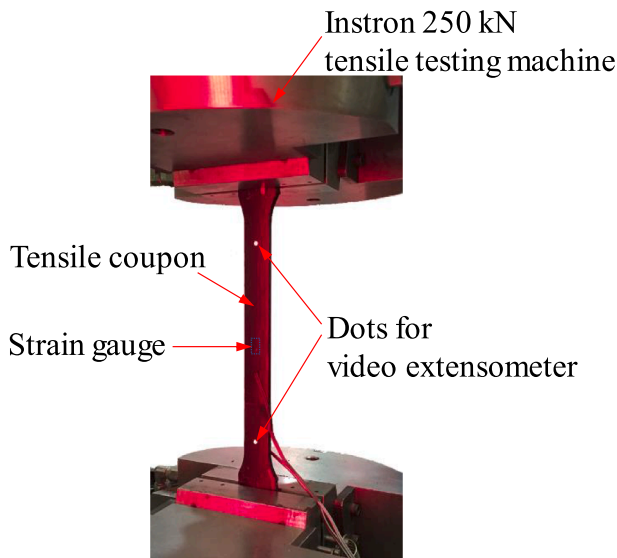


Fig. 2. Tensile coupon test setup.

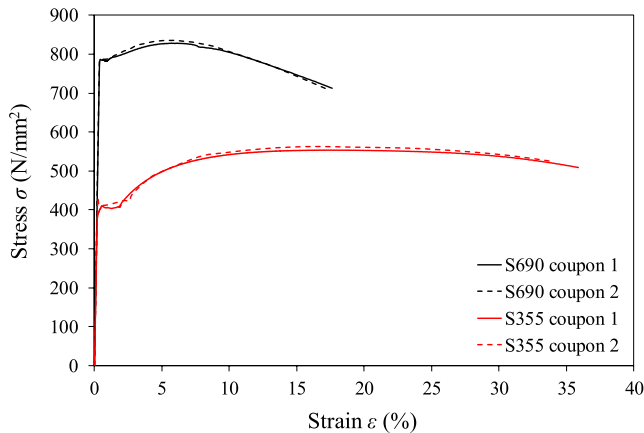


Fig. 3. Measured stress-strain curves from tensile coupon tests.

Table 1
Chemical composition of S355 and S690 steels used in the present study.

Steel grade	C %	Si %	Mn %	P %	S %	N %	Cu %	Mo %	Ni %	Cr %	V %	Nb %	Ti %	B %	Zr %	Al %
S355	0.165	0.475	1.548	0.013	0.0008	–	0.023	0.01	0.029	0.031	0.001	–	–	–	–	0.042
S690	0.139	0.284	1.436	0.013	0.0007	0.0029	0.026	0.068	0.029	0.323	0.002	0.022	0.011	0.0016	0.0002	0.031

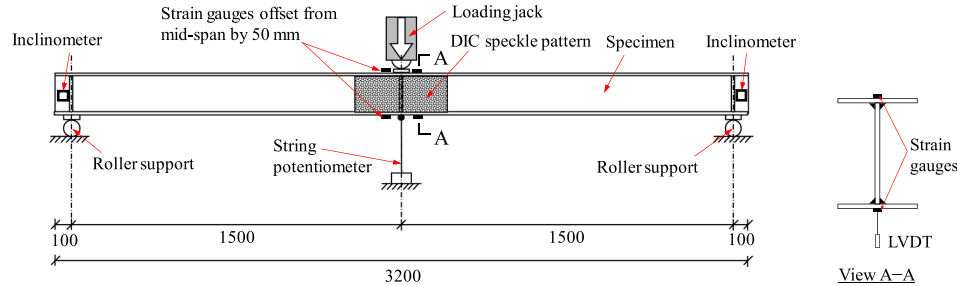
bending considering web-flange interaction. More recently, the in-plane flexural behaviour of S690 HSS welded I-section beams was investigated by Sun et al. [13], confirming the general accuracy of the Class 2 and Class 3 slenderness limits set out in EN 1993-1-12 [14] for S690 HSS welded I-sections in bending. However, the restrictions regarding the plastic design of HSS structures, as specified in EN 1993-1-12 [14], were questioned by Bartsch et al. [15] who examined the rotation capacity of HSS welded I-section beams experimentally and verified that HSS beams were capable of attaining their plastic moment resistances and exhibiting good rotation capacities. Bending tests on HSS tubular elements also demonstrated high levels of ductility [16–18]. With regards to hybrid welded I-sections, Suzuki et al. [19] carried out a series of physical tests on simply-supported beams with an HSS web and NSS flanges, observing that the plastic deformation capacity of such hybrid beams was greater than that of their homogeneous HSS counterparts. Shokouhian and Shi [20] conducted both experimental and numerical investigations into the flexural strength of hybrid steel I-section beams with Q460 steel flanges and a Q345 steel web subjected to uniform bending moment, and proposed a slenderness based method to determine their flexural strengths considering the effects of local buckling, global buckling and the interaction between the two. Shokouhian and Shi [21] also studied the influence of flange and web slenderness on the ductility of beams made of HSS homogeneous and hybrid welded I-sections, revealing that stricter GB 50017 [22] flange and web slenderness limits are required for these beams to achieve a rotation capacity of $R_{req} = 3$, which was adopted as the minimum requirement for plastic design in the development of Eurocode 3 [23] and AISC 360 [24].

The current design provisions given in EN 1993-1-12 [14] for HSS structures with steel grades up to S700 generally follow the design of NSS structures in EN 1993-1-1 [23], but with some restrictions. In the context of cross-section classification and design, the slenderness limits for HSS cross-sections are the same as those for NSS cross-sections, but plastic design is currently not permitted for HSS structures. The objectives of the present study are, therefore, to evaluate the accuracy of the current Eurocode slenderness limits for application to HSS homogeneous and hybrid welded I-sections and to assess the potential use of plastic design for HSS structures in light of a newly assembled pool of experimental and numerical results.

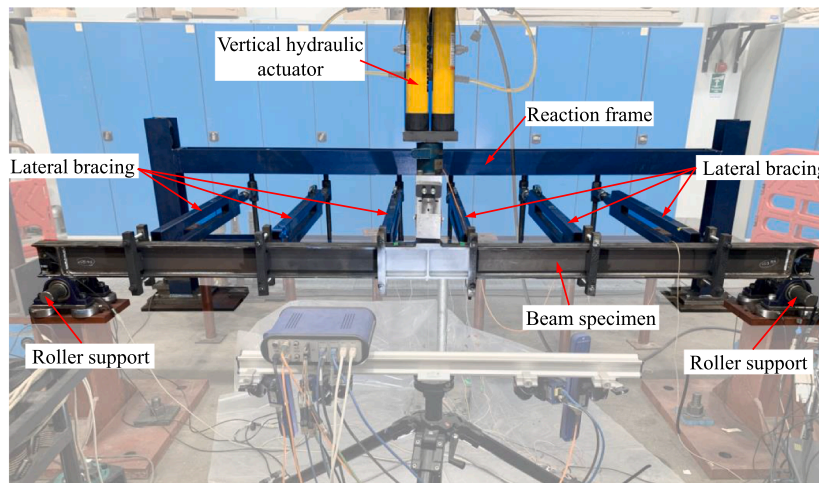
The present investigation features experimental, numerical and design-oriented studies into HSS beams. A total of six in-plane three-point bending tests on HSS homogeneous and hybrid welded I-sections are first described in Section 2. Three different I-sections – two

Table 2
Key average material properties for S355 and S690 steels from tensile coupon tests.

Steel grade	E	f_y	f_u	ϵ_y	ϵ_{sh}	ϵ_u	ϵ_f	f_u/f_y	ϵ_u/ϵ_y
S355	N/mm ² 198,500	N/mm ² 404.1	N/mm ² 553.5	% 0.20	% 1.89	% 17.22	% 34.8	– 1.37	– 84.6
S690	N/mm ² 212,000	N/mm ² 782.5	N/mm ² 828.4	% 0.37	% 0.96	% 6.17	% 17.3	– 1.06	– 16.7



(a) Schematic diagram (dimensions in mm)



(b) Lateral restraint system

Fig. 4. Configuration of beam specimens and experimental setup for major axis three-point bending tests.

Table 3
Average measured geometrical dimensions and cross-sectional properties of beam specimens.

Beam specimen	L mm	L_{span} mm	B mm	H mm	t_f mm	t_w mm	A mm ²	I mm ⁴	W_{el} mm ³	W_{pl} mm ³	M_{el} kNm	M_{pl} kNm
HSS-I-65 × 116 × 8 × 8-3 PB	3200	3000	64.42	116.31	8.40	8.45	1985.8	3.995×10^6	6.869×10^4	7.112×10^4	54.03	64.74
HSS-I-65 × 116 × 8 × 8-3 PB-R	3200	3000	62.22	116.50	8.40	8.42	1947.5	3.900×10^6	6.695×10^4	6.938×10^4	52.66	63.26
HSS-I-80 × 136 × 8 × 8-3 PB	3200	3000	79.59	136.67	8.41	8.43	2411.8	6.934×10^6	1.015×10^5	1.044×10^5	79.81	94.20
HSS-I-80 × 136 × 8 × 8-3 PB-R	3200	3000	79.42	136.75	8.44	8.44	2415.0	6.949×10^6	1.016×10^5	1.046×10^5	79.93	94.36
HYB-I-80 × 136 × 8 × 8-3 PB	3200	3000	79.71	136.72	8.40	8.08	2370.8	6.893×10^6	1.008×10^5	1.036×10^5	75.53	80.99
HYB-I-80 × 136 × 8 × 8-3 PB-R	3200	3000	79.61	136.65	8.37	8.18	2376.3	6.877×10^6	1.006×10^5	1.035×10^5	75.34	80.79

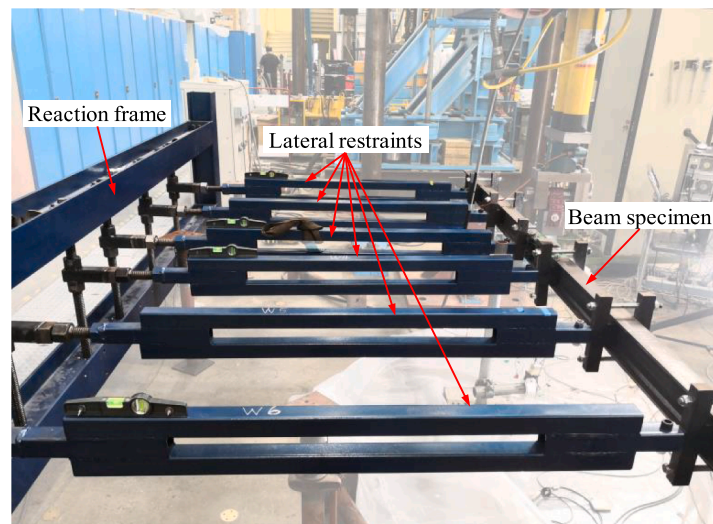
homogeneous S690 steel welded I-sections and one hybrid welded I-section with S690 steel flanges and an S355 steel web, were adopted in the experimental programme. The beam specimens were bent about the major axis and a bespoke restraint rig was employed to prevent out-of-plane instability. Following the experimental study, finite element (FE) models were established and validated against the test results obtained from the present study as well as those collected from the literature [13], as described in Section 3. The validated FE models were used to perform a series of parametric studies to generate supplementary numerical data on HSS homogeneous and hybrid welded I-section beams, covering a wide range of cross-section aspect ratios, cross-section slendernesses, loading configurations and steel grades. Based on the obtained test and

FE results, the rotation capacity of HSS homogeneous and hybrid welded I-section beams was investigated and the suitability of the current Eurocode slenderness limits [14] was assessed.

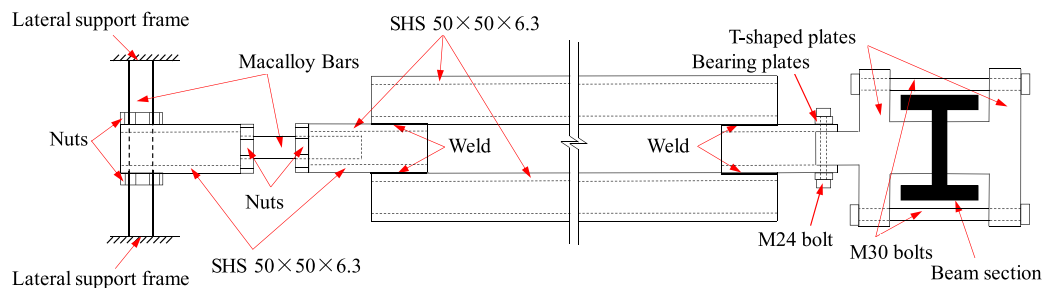
2. Experimental programme

2.1. General

An experimental study was performed to investigate the major-axis flexural behaviour and rotation capacity of HSS homogeneous and hybrid welded I-section beams subjected to mid-span concentrated load. Specifically, a total of six three-point major axis bending tests, with two



(a) Photo



(b) Schematic drawing

Fig. 5. Lateral restraint system for three-point bending tests.

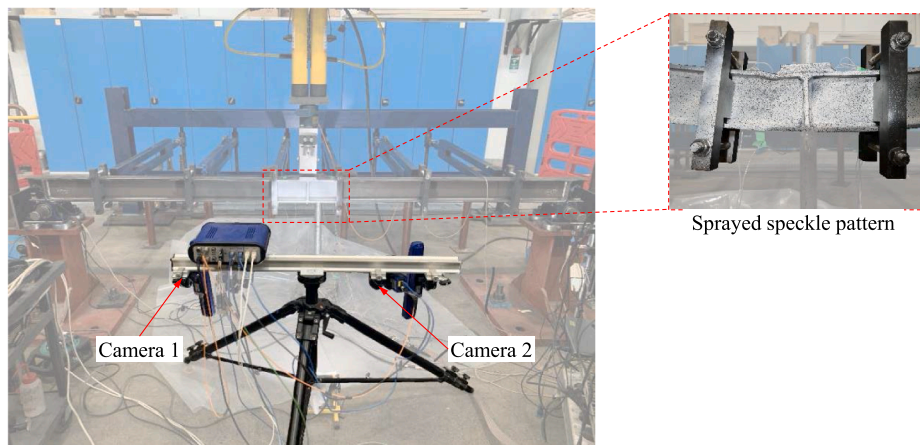


Fig. 6. DIC setup and speckle pattern for three-point bending tests.

on each of the three investigated welded I-section profiles (i.e. HSS-I-65 × 116 × 8 × 8, HSS-I-80 × 136 × 8 × 8 and HYB-I-80 × 136 × 8 × 8), were conducted. Three-point bending tests were chosen to investigate the bending resistance and rotation capacity of the studied cross-sections under a moment gradient; this is a common scenario in plastic designed frames. Each beam specimen was labelled by a unique identifier, e.g. HSS-I-65 × 116 × 8 × 8-3 PB, where HSS-I (or HYB-I) denotes a homogeneous HSS welded I-section made of S690 steel for both its flanges and web (or a hybrid welded I-section with its flanges made of S690 steel and web made of S355 steel), 65 × 116 × 8 × 8 are

the nominal dimensions of the welded I-section in millimetres (i.e. flange width B × outer section height H × flange thickness t_f × web thickness t_w) as illustrated in Fig. 1 and 3 PB represents three-point bending tests. For repeated tests, the letter “R” is added as a suffix to the specimen identifier. All three welded I-section sizes were fabricated from 8 mm-thick quenched and tempered S690 steel plates and hot-rolled S355 steel plates by means of gas metal arc welding with a nominal weld leg length (t_{weld}) of 5.6 mm (i.e. a weld throat thickness of 4 mm), as shown in Fig. 1.

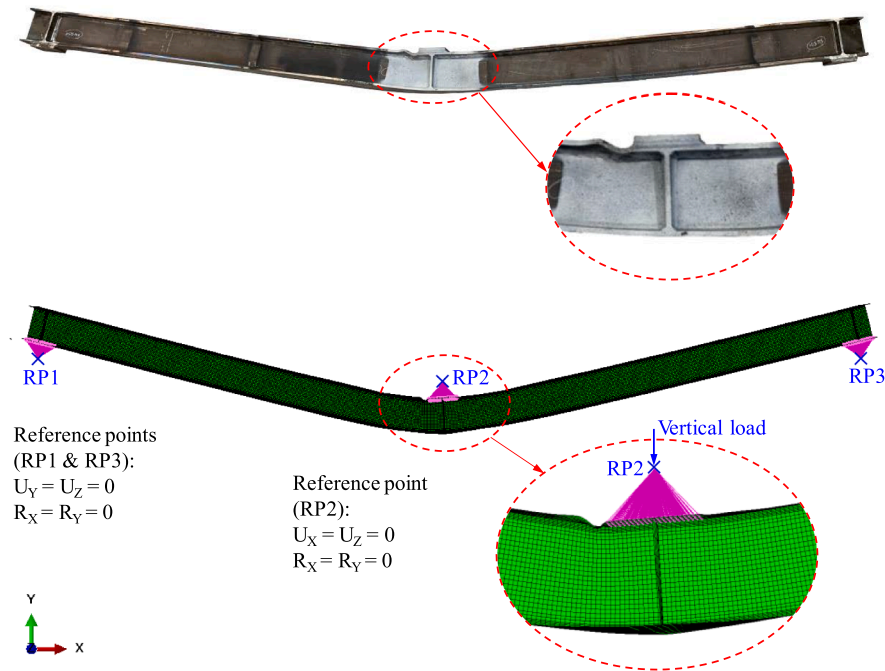


Fig. 7. Comparison between test and FE failure modes for HYB-I-80 × 136 × 8 × 8-3 PB.

2.2. Material testing and geometry measurements

The chemical composition of the two examined steel grades (S355 and S690) used in the present study, as provided by the manufacturer, are reported in Table 1, which are shown to satisfy the requirements specified in EN 10025-2 [25] for hot-rolled S355 steel and EN 10025-6 [26] for quenched and tempered S690 steel. Prior to the bending tests, tensile coupon tests were conducted to obtain the key material properties and full-range stress–strain responses of the investigated steels. For each of the two examined steel grades (S355 and S690), two tensile coupons were extracted from the same batch of steel plates used to fabricate the beam specimens, along the rolling direction. The geometrical dimensions of the coupon specimens were in compliance with the requirements specified in EN ISO 6892-1 [27]. The tensile coupons were tested using an Instron hydraulic 250 kN testing machine under displacement control, with a constant displacement rate of 0.05 mm/min for the elastic range and a higher rate of 0.5 mm/min for the subsequent post-yield range of the stress–strain curves. A video extensometer was installed to measure the elongation over a gauge length of 140 mm, and two strain gauges were affixed to each side of the coupons at mid-height to measure the longitudinal tensile strain, as shown in Fig. 2.

The measured full-range stress–strain curves for the two steel grades are shown in Fig. 3, while the key average material properties for each steel grade are reported in Table 2, where E is the Young's modulus, f_y is the yield strength, f_u is the ultimate strength, ϵ_y is the yield strain, ϵ_{sh} is the strain hardening strain, ϵ_u is the strain corresponding to the ultimate strength, and ϵ_f is the strain at fracture (i.e. measured over a gauge length of 140 mm). It can be observed from Fig. 3 that the stress–strain curves for the S690 steel exhibit a shorter yield plateau, a less pronounced level of strain hardening and reduced ductility in comparison with the S355 steel; this is also reflected in the key average material properties given in Table 2.

The nominal length of all beam specimens L was 3200 mm, with an overhang of 100 mm at each end beyond the corresponding roller

support, resulting in a span of $L_{span} = 3000$ mm for each tested specimen, as illustrated in Fig. 4(a). The average measured geometrical dimensions for each beam specimen are reported in Table 3, together with the cross-sectional properties calculated based on the measured dimensions, where A is the cross-sectional area, I is the second moment area about the major axis, W_{el} and W_{pl} are the elastic and plastic section moduli about the major axis, respectively, and M_{el} and M_{pl} are the elastic and plastic bending moment capacities about the major axis, respectively. Note that, in Table 3, M_{el} for the hybrid welded I-sections is defined as the bending moment at which the stress at the extreme outer-fibre of the flange reaches its yield strength, as detailed further in Section 4.6. The three investigated welded I-sections are all Class 1 cross-sections under pure bending according to the slenderness limits specified in prEN 1993-1-1: 2018 [28].

2.3. Three-point bending tests

A schematic view of the arrangement of the test rig and the instrumentation for the three-point in-plane bending tests is shown in Fig. 4 (a). Each beam specimen was simply supported between a pair of steel rollers, which permitted the beam ends to undergo rotations about the axis of bending as well as longitudinal displacements. The tested beam specimens were loaded at mid-span using an Instron 250 kN testing machine under displacement control at a vertical displacement rate of 2.0 mm/min. Stiffeners and bearing plates were welded at the mid-span and the ends of the beam specimens to prevent web crippling under concentrated transverse loading.

A bespoke lateral restraint system was designed and employed to prevent lateral and torsional deformations of the beam specimens and hence to prevent lateral-torsional buckling (LTB). The lateral restraint system was composed of a reaction frame and six lateral restraints, as shown in Fig. 4(b). Each lateral restraint comprised two T-shaped plates which were used to clamp the section of the beam specimen by means of two M30 bolts, and a bracing beam made of two parallel S460 square hollow section (SHS) members, as illustrated in Fig. 5. The assembled T-

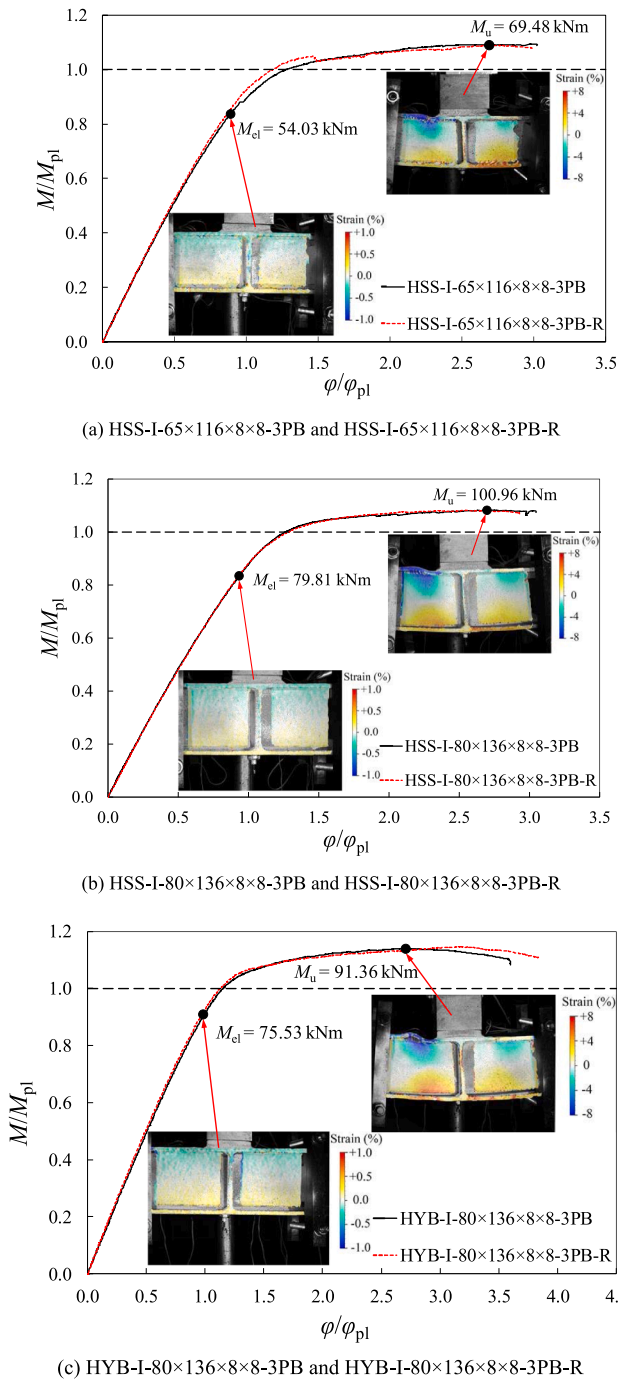


Fig. 8. Normalised mid-span bending moment-mid-span rotation curves and longitudinal strain fields at different representative loads obtained from DIC for three-point bending specimens.

Table 4
Key experimental results from three-point bending tests.

Specimen	M_u kNm	M_u/M_{pl}	φ_{pl} rad	φ_u rad	R
HSS-I-65 × 116 × 8 × 8-3 PB	69.48	1.05	0.11	0.35	>2.14
HSS-I-65 × 116 × 8 × 8-3 PB-R	67.50	1.05	0.11	0.35	>2.23
HSS-I-80 × 136 × 8 × 8-3 PB	100.96	1.05	0.10	0.30	>1.93
HSS-I-80 × 136 × 8 × 8-3 PB-R	100.91	1.05	0.11	0.28	>1.67
HYB-I-80 × 136 × 8 × 8-3 PB	91.36	1.12	0.09	0.30	>2.50
HYB-I-80 × 136 × 8 × 8-3 PB-R	90.78	1.11	0.08	0.32	>2.91

shaped plates were bolted to the bracing beam with an M24 bolt, the shank of which was greased to facilitate free rotation. Each lateral restraint was connected to the reaction frame via two 35 mm-diameter Macalloy bars as shown in Fig. 5, enabling the lateral restraint to be adjustable in both length and height. During testing, a ratchet spanner was employed to rotate the threaded bars installed in the reaction frame in order to adjust the height of the lateral restraints to match the corresponding vertical deflections of the beam specimens. The same lateral restraint system has also been successfully employed in previous HSS frame tests [29].

Four strain gauges were affixed to the top and bottom flanges of the beam sections, at a distance of 50 mm from the stiffened mid-span section, as shown in Fig. 4(a), to monitor the strain development histories during testing. A string potentiometer was attached to the bottom flange of the beam at mid-span to record the vertical deformation of the beam during loading. Two inclinometers were mounted onto the webs of the extended overhangs to record the end rotations about the bending axis. The test outputs, including the applied vertical load and readings from the strain gauges, string potentiometer and inclinometers were recorded at 2-second intervals using the data acquisition equipment DATASCAN.

To gain further insight into the strain development at the mid-span region of the beam specimens where inelastic local buckling occurred, in addition to the traditional instrumentation described above, a two-camera digital image correlation (DIC) system was employed. The DIC setup is shown in Fig. 6, where two cameras, with the focal lengths set to 35 mm, were utilised for the image acquisition. Prior to testing, the mid-span region of all beam specimens was painted white and then sprayed with a random black speckle pattern, as shown in Fig. 6. Images were taken at 2-second intervals and processed using the DaVis version 8.4.0 imaging software [30].

All the tested beam specimens failed by inelastic local buckling in the maximum moment region adjacent to the stiffened mid-span, a typical example of which is shown in Fig. 7. The normalised mid-span bending moment (M)-mid-span rotation (φ) curves for all tested beam specimens are plotted in Fig. 8, where the mid-span bending moment M was calculated from the applied vertical load, with allowance for the horizontal movement at the supports [18], and the mid-span rotation φ was determined as the sum of the end rotations recorded by the two inclinometers at the overhangs, as shown in Fig. 4(a). The key test results are summarised in Table 4, where M_u is the ultimate bending moment at mid-span, φ_{pl} is the elastic component of the mid-span rotation when M_{pl} is first attained, determined by Eq. (1), φ_u is the mid-span rotation at M_u and R is the rotation capacity. The rotation capacity R is defined by Eq. (2), where φ_{rot} is the mid-span rotation when the moment at mid-span falls below M_{pl} on the descending branch. Note that the maximum recorded rotation φ_{max} , instead of φ_{rot} , was employed in Eq. (2) to calculate the rotation capacities of the presented three-point bending tests since these tests exceeded their peak moments, but were discontinued prior to the bending moment dropping below M_{pl} ; the obtained rotation capacities, as listed in Table 4 may therefore be considered to be lower bounds.

$$\varphi_{pl} = \frac{M_{pl}L_{span}}{2EI} \quad (1)$$

$$R = \frac{\varphi_{rot}}{\varphi_{pl}} - 1 \quad (2)$$

With regards to beams subjected to four-point bending, the results of which have been collected from the literature and generated in the FE parametric study described later, the curvature in the constant moment region was utilised for calculating the rotation capacity, as given by Eq. (3), where κ_{pl} is the elastic curvature corresponding to the plastic bending moment M_{pl} and κ_{rot} is the curvature when the mid-span bending moment falls below M_{pl} on the descending branch. The curvature is defined based on the assumption that the deformed shape of the

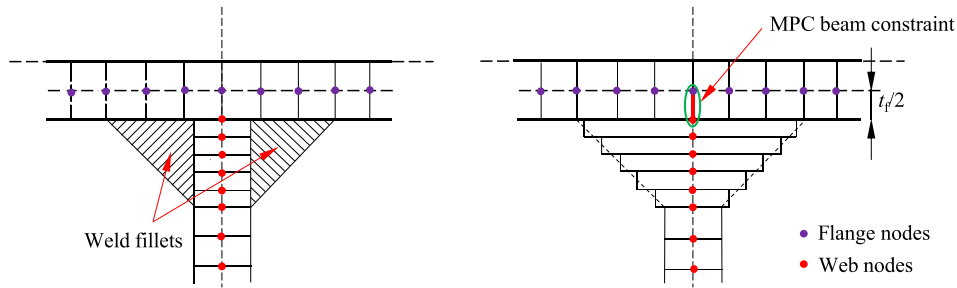


Fig. 9. Illustration of modelling technique for accurately representing the geometry of the welded I-sections.

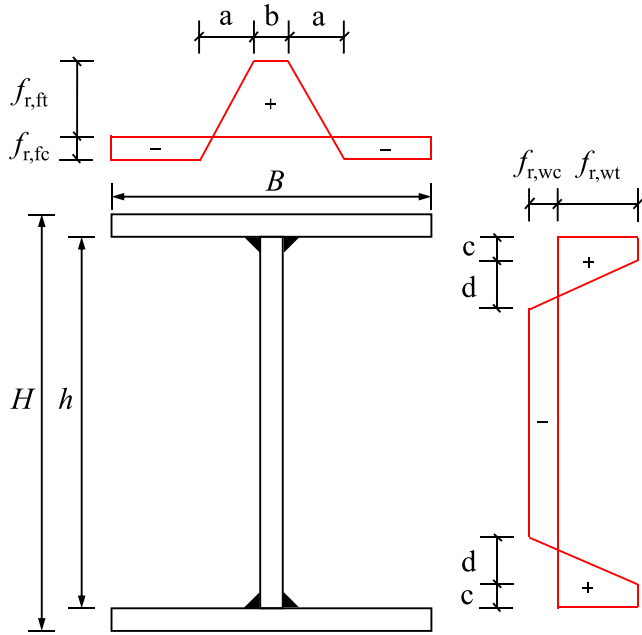


Fig. 10. Proposed residual stress pattern [38].

Table 5
Residual stress pattern for NSS and HSS steel welded I-sections.

$f_{r,wt} = f_{r,ft}$	$f_{r,wc} = f_{r,fc}$	a	b	c	d
Eq. (5) or Eq. (6)	From equilibrium	0.1B	0.14B	0.07 h	0.1 h

constant moment region (i.e. the mid-region between two loading points) represents a segment of a circular arc (of radius r), resulting in the expression of Eq. (4), where D_M is the vertical displacement at mid-span and D_L is the average vertical displacement at the two loading points. This definition of rotation capacity for beams in four-point bending has been employed in many previous studies [17,18].

$$R = \frac{\kappa_{rot} - 1}{\kappa_{pl}} \quad (3)$$

$$\kappa = \frac{8(D_M - D_L)}{4(D_M - D_L)^2 + L_M^2} \quad (4)$$

The accuracy of the measurements obtained from the DIC system has been confirmed by comparing the displacement and strain histories obtained from the DIC system to those measured from the string potentiometers and strain gauges, respectively, at the corresponding location of each beam specimen. A more detailed description of the DIC validation has been reported by Yun et al. [29]. The longitudinal strain fields within the mid-span regions of beam specimens HSS-I-65 × 116 × 8 × 8-3 PB, HSS-I-80 × 136 × 8 × 8-3 PB and HYB-I-80 × 136 × 8 ×

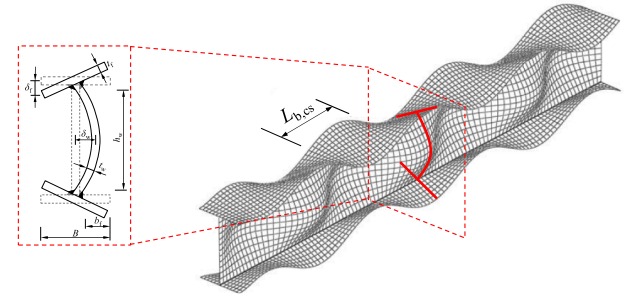


Fig. 11. Definition of shape and amplitude of local geometric imperfections (not to scale) employed in FE models.

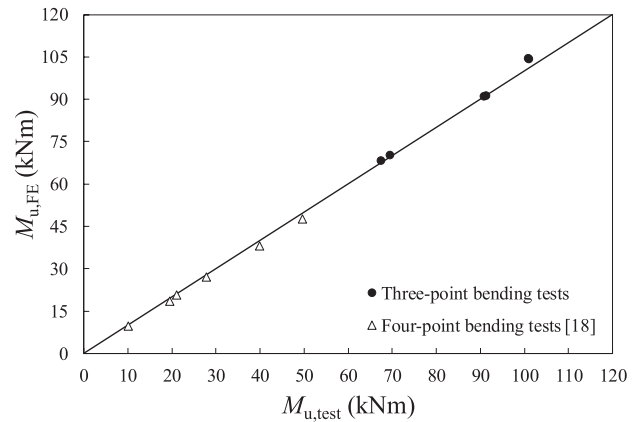


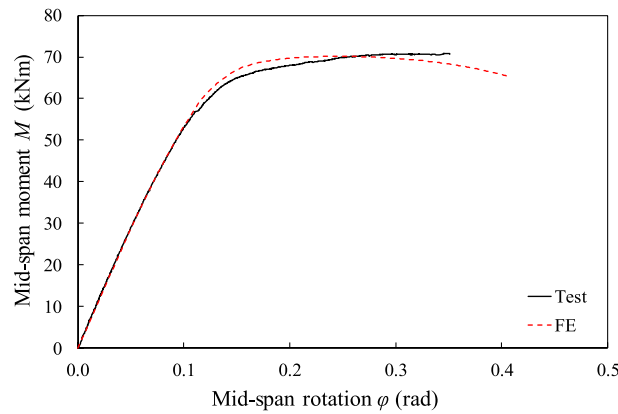
Fig. 12. Comparison between ultimate bending moments obtained from FE models $M_{u,FE}$ and tests $M_{u,test}$.

8-3 PB, obtained from the DIC analyses at two representative load levels: (1) the load at which the mid-span bending moment reached the elastic bending moment M_{el} , and (2) the maximum applied load corresponding to M_u , are displayed in Fig. 8, where the development of the inelastic local buckling can be observed. Note that the positive and negative strains in Fig. 8 represent tensile strains and compressive strains, respectively.

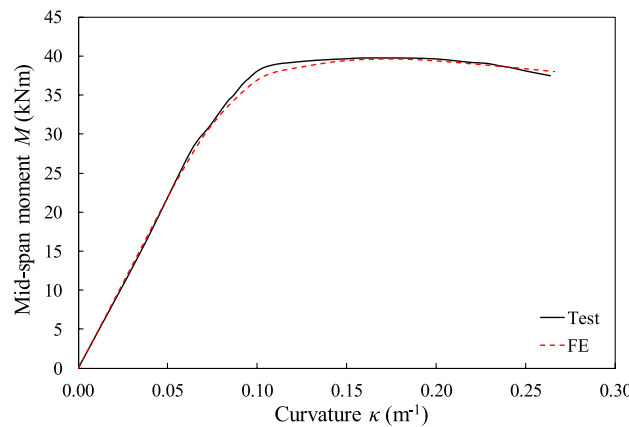
3. Numerical simulations

3.1. General

In parallel with the experimental studies, comprehensive numerical simulations were performed to investigate the in-plane flexural behaviour of HSS homogeneous and hybrid welded I-section beams using the finite element (FE) analysis software ABAQUS [31]. The basic modelling assumptions and validation of the FE models are described in Section 3.2



(a) Three-point bending test carried out in the present study (HSS-I-65×116×8×8-3PB)



(b) Four-point bending test carried out by Sun et al. (I-100×100×5-MA) [13]

Fig. 13. Typical comparisons between moment-deformation curves obtained from tests and FE models.

Table 6
Summary of key material properties for S355, S460 and S690 steels employed in parametric studies.

Steel grade	E	f_y	f_u	f_u/f_y	ϵ_u	ϵ_{sh}
	N/mm ²	N/mm ²	N/mm ²	–	–	–
S355	210,000	355	490	1.38	0.17	0.017
S460	210,000	460	540	1.17	0.09	0.030
S690	210,000	690	770	1.12	0.06	0.030

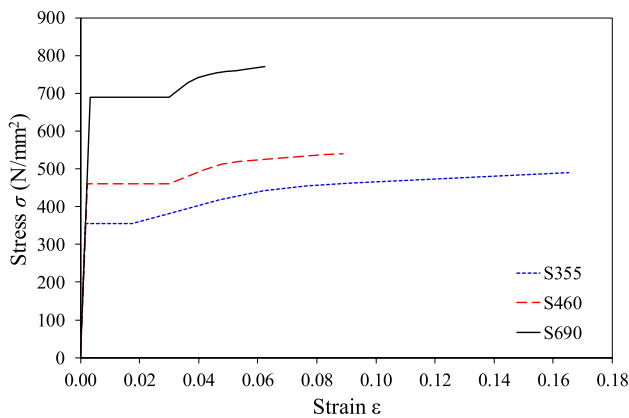


Fig. 14. Full-range stress–strain curves for S355, S460 and S690 steels employed in parametric studies [42].

and Section 3.3, respectively, while parametric studies, which were carried out to generate further numerical data considering different key parameters, are presented in Section 3.4.

3.2. Basic modelling assumptions

The four-noded shell element S4R with reduced integration and finite membrane strains was used for all simulations in the present study; this element has been shown to be capable of modelling the buckling behaviour of plated structural elements and has been successfully employed in several previous studies on I-sections subjected to different loading conditions [32–34]. The FE models were validated against the three-point bending tests performed in the present study, as well as the four-point bending tests reported in [13]. The measured stress–strain curves transformed into true stress–logarithmic plastic strain curves for incorporation into ABAQUS [31], were used in both cases.

The measured average cross-sectional dimensions of the welded I-sections of each beam specimen were carefully modelled using the following technique: (1) the nodes at each end of the web, offset from the centreline of the flange by half the flange thickness to avoid overlap between the flange and web plates, were coupled to their corresponding nodes at the mid-thickness of the flanges using *MPC BEAM constraints, and (2) each web-to-flange fillet weld zone, with the shape of each fillet weld assumed to be a right-angled triangle, was represented by five equal-height web elements, which were assigned different thicknesses according to the measured dimensions, as shown in Fig. 9. The nominal weld leg length of 5.6 mm was employed in the validation FE models. In the transverse direction, a mesh size of approximately $(B + H)/40$ was adopted in the flange and web plates; the same mesh size was also

Table 7
Ranges of variation of parameters considered in parametric studies.

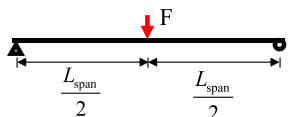
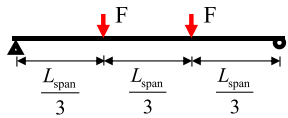
Loading configuration	Material combination (Flange / Web)	B mm	H mm	t_f mm	t_w mm	t_{weld} mm	L_{span} mm
 <p>Three-point bending</p>	S690 / S690	100	100/150/200/300	3.4–17	0.6 t_f	5.6	15H
	S460 / S460						
	S355 / S355						
	S690 / S355						
	S690 / S355						
 <p>Four-point bending</p>	S690 / S690	100	100/150/200/300	3.4–17	0.6 t_f	5.6	15H
	S460 / S460						
	S355 / S355						
	S690 / S355						
	S690 / S355						

Table 8
Summary of existing bending tests on homogeneous and hybrid welded I-section beams.

Cross-section type	Loading configuration	Steel grade/flange (web)	Number of tests	References
Homogeneous	3 PB	S690	4	Present study
	4 PB	S700	10	[12]
	4 PB	S690	6	[13]
	3 PB	S355/S690	10	[15]
	4 PB	Q345 ^a	3	[20]
	3 PB/4PB	SM490 ^b / HSB800 ^b / HSA800 ^b	21	[43]
	3 PB/4PB	S700/S960	8	[44]
	3 PB	Q550 ^a	6	[45]
	4 PB	Q460 ^c /Q890 ^c	5	[46]
	3 PB	S690(S355)	2	Present study
Hybrid	3 PB	S690(S355)	10	[15]
	4 PB	Q460 ^a (Q345 ^a)	3	[20]
	3 PB/4PB	HPS485W ^d (Q235 ^e / Q345 ^a)	13	[47]

Note. ^a Specified according to GB/T 1591–2008 [48]; ^b Specified according to JIS G3106-1999 [49]; ^c Specified according to GB/T 16270–2009[50]; ^d Specified according to ASTM A709 / A709M-18 [51]; ^e Specified according to GB/T 700–2006 [52].

assigned uniformly in the longitudinal direction of the modelled beam specimens, such that the element aspect ratio was close to unity. The mesh size was selected based on a prior mech sensitivity study, where mesh sizes ranging between $(B + H)/100$ and $(B + H)/20$ were examined. A mesh size of $(B + H)/40$ which provided accurate results at reasonable computational cost, was finally selected to discretize the FE models.

Welding induces residual stresses into fabricated structural steel sections, typically leading to the earlier onset of yielding and a reduction in load-carrying capacity. Residual stresses in both NSS and HSS welded I-sections have been investigated in a number of previous studies [35–37]. Recently, Yun et al. [38] collected available residual stress data on welded I-sections from the literature and proposed predictive models for the residual stress pattern in both NSS and HSS welded I-sections, as shown in Fig. 10. Table 5 summarises the parameters employed in the proposed model, where $f_{r,wt}$ and $f_{r,ft}$ are the maximum tensile residual stresses in the web and the flanges, respectively, $f_{r,wc}$ and $f_{r,fc}$ are the maximum compressive residual stresses in the web and the flanges, respectively, while stress distribution dimensions a, b, c and d are defined in Fig. 10.

The maximum tensile residual stresses can be determined from Eq. (5) or Eq. (6), which correspond to the mean or upper characteristic (i.e. 95 percentile) values from the analysed experimental database [38],

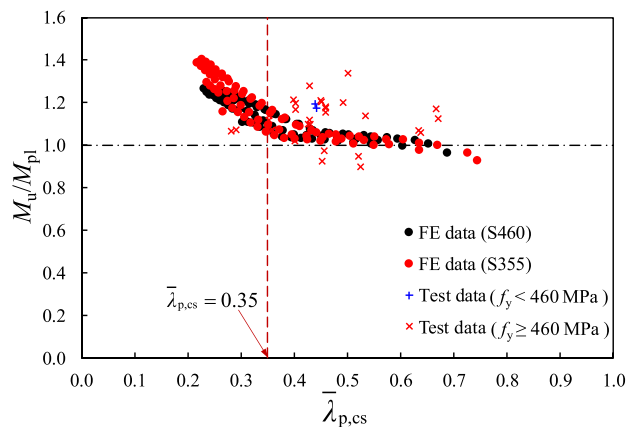
respectively. Note that for welded I-sections whose flange plates are flame-cut, the tips of the flanges are left in residual tension; the beneficial effect of the tensile residual stresses induced by flame-cut was, however, not considered in the proposed model.

$$\frac{f_{r,wt}(f_{r,ft})}{f_y} = -0.5 \times \sqrt{\frac{f_y}{235}} + 1.32 \leq 1 \quad (5)$$

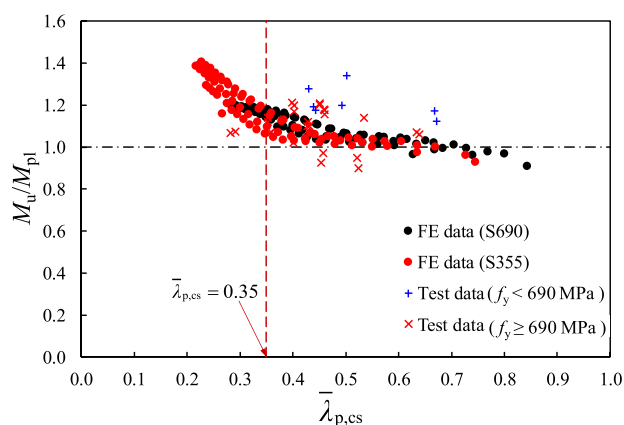
$$\frac{f_{r,wt}(f_{r,ft})}{f_y} = -0.5 \times \sqrt{\frac{f_y}{235}} + 1.5 \leq 1 \quad (6)$$

It was recommended by Yun et al. [38] that the proposed residual pattern, using the mean value of the maximum tensile residual stress (i.e. Eq. (5)) is used for the validation of FE models (to match test results), while the proposed residual pattern with the upper characteristic value of the maximum tensile residual stress (i.e. Eq. (6)) is employed for parametric studies (to provide safe-sided capacity data). This approach is adopted in the present study. The proposed residual stress pattern is also deemed suitable for the prediction of residual stress distributions in hybrid welded I-sections consisting of steel plates of different steel grades. For hybrid welded I-sections, the maximum tensile residual stresses in the web $f_{r,wt}$ and the flanges $f_{r,ft}$ should also be determined using Eq. (5) or Eq. (6), but with the value of f_y taken as the greater yield strength of the constituent plates. In cases that the calculated maximum tensile residual stress exceeds the yield strength of the corresponding plate, the maximum tensile residual stress should be taken equal to the yield strength of that plate. The membrane residual stresses determined from the proposed pattern [38] were incorporated into the developed FE models as an initial stress condition using the ABAQUS command *INITIAL CONDITIONS.

Initial geometric imperfections were introduced into the developed FE models by modifying the nodal coordinates of the perfect geometry. Local geometric imperfections were assigned to the FE models in a sinusoidal shape with a half-wavelength $L_{b,cs}$ [39], as shown in Fig. 11. The local imperfection half-wavelength $L_{b,cs}$ was set equal to the elastic local buckling half-wavelength of the welded I-section in compression, which was determined using the finite strip software CUFSM [40], ensuring that an integer number of half-wavelengths were fitted within the member length. The magnitudes of the local geometric imperfections were taken as the tolerance-based values recommended in Annex C of EN 1993-1-5 [41]. Specifically, the magnitude of the local web imperfection δ_w was taken equal to $1/200$ of the clear height of the web h_w (i.e. $h_w = H - 2t_f - 2t_{weld}$) when the elastic local buckling stress of the web plate in pure compression $\sigma_{cr,w}$ was less than or equal to that of the flange plates $\sigma_{cr,f}$ (i.e. the web plate was more susceptible to local buckling compared to the flange plates), while the magnitude of the local flange imperfection δ_f was taken as $1/50$ of the clear width of each flange outstand b_f (i.e. $b_f = (B - t_w)/2 - t_{weld}$) when $\sigma_{cr,f} < \sigma_{cr,w}$, which indicates that the web plate was less susceptible to local buckling than the flange plates. By assuming the web-to-flange junctions of the welded



(a) Comparison of normalised ultimate bending capacity (M_u/M_{pl}) of S460 and S355 steel beams in three-point bending



(b) Comparison of normalised ultimate bending capacity (M_u/M_{pl}) of S690 and S355 steel beams in three-point bending

Fig. 15. Influence of material grade on normalised ultimate bending moment M_u/M_{pl} of welded I-section beams in three-point bending.

I-sections remained at 90 degrees, the local imperfection amplitude of the non-critical plate (i.e. the plate with the higher elastic local buckling stress) can be defined, as illustrated in Fig. 11. The use of tolerance-based imperfection amplitudes would be expected to yield slightly conservative resistance predictions in comparison to experimental results.

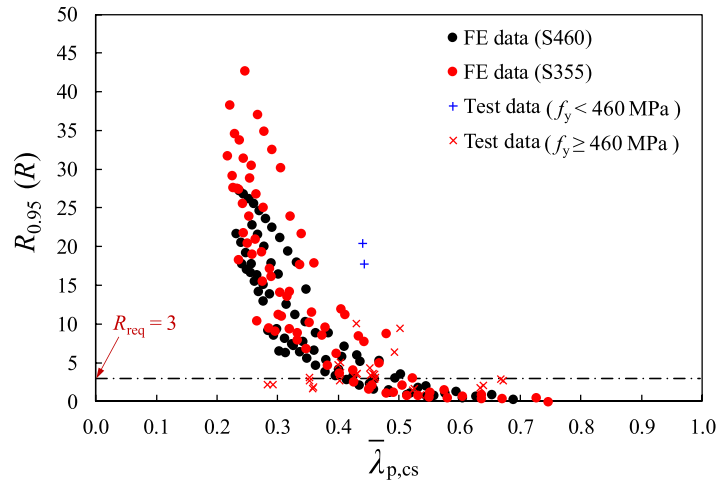
Suitable boundary and loading conditions were employed in the FE models to mimic the corresponding test setup, as described in Section 2.3 for the three-point bending tests and reported in [13] for the four-point bending tests. All degrees of freedom of the upper (i.e. for the loading points) or lower (i.e. for the support points) flange nodes over a region corresponding to the location of the bearing plates (or wooden blocks [13]) employed in the tests were coupled to a corresponding reference point, where the boundary and loading conditions were assigned, as detailed in Fig. 7. Stiffeners were also modelled at the loading and support sections where concentrated loads were applied in order to prevent localised web crippling failure, as employed in the tests. The stiffeners were tied to their corresponding cross-sections using *TIE constraints, and their material properties were assumed to be the same as those of the corresponding flange plates. The out-of-plane displacement degree of freedom of the nodes located at the cross-sections where lateral restraints were provided was also constrained to prevent lateral-torsional buckling. The modified Riks method was employed for the geometrically and materially nonlinear analyses (GMNIA), enabling the post-ultimate response of the modelled specimens to be tracked.

3.3. Validation of FE models

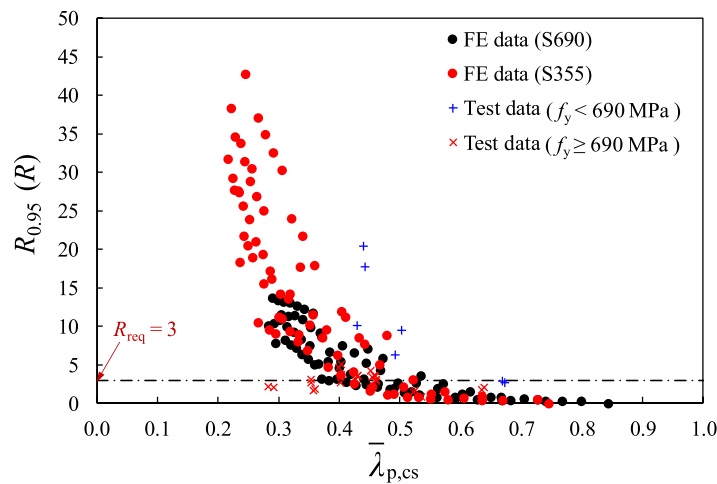
The developed FE models were validated against the results from the three-point bending tests described in Section 2.3 and the four-point bending tests reported in [13] in terms of ultimate bending moments, full moment-deformation histories and failure modes. The ultimate bending moments derived from the FE models $M_{u,FE}$ are plotted against the results from the three-point and four-point bending tests $M_{u,test}$ in Fig. 12, indicating good agreement, with the mean value of the ratio of $M_{u,test}/M_{u,FE}$ being 0.98 and the corresponding coefficient of variation being 0.02. The experimental moment-deformation curves and failure modes were also well replicated by the FE models, as illustrated by the typical examples displayed in Figs. 13 and 7, respectively. It can thus be concluded that the established FE models are capable of replicating the flexural behaviour of the homogeneous and hybrid HSS welded I-section beams subjected to major axis bending.

3.4. Parametric studies

Upon the validation of the developed FE models, parametric studies were conducted with the aim of expanding the experimental data pool for homogeneous and hybrid welded I-section beams over a wide range of cross-section aspect ratios, cross-section slendernesses, steel grades and loading configurations. Regarding the geometry of the modelled I-sections, the flange width B was kept constant at 100 mm, while four outer section heights H of 100, 150, 200 and 300 mm were considered,



(a) Comparison of rotation capacity of S460 and S355 steel beams in three-point bending



(b) Comparison of rotation capacity of S690 and S355 steel beams in three-point bending

Fig. 16. Influence of material grade on rotation capacity of welded I-section beams in three-point bending.

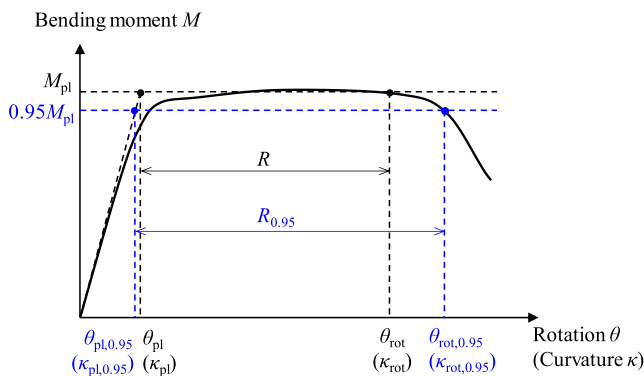
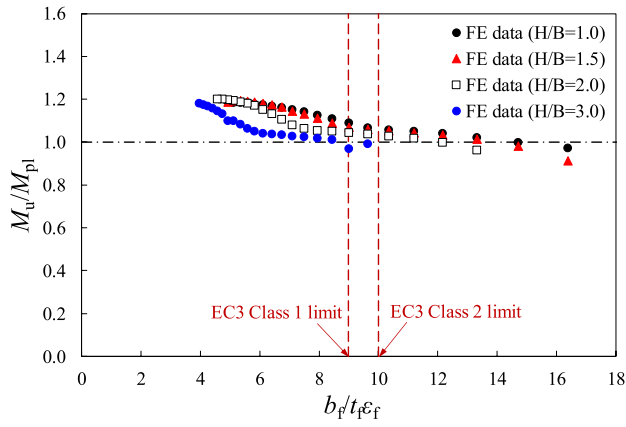


Fig. 17. Definition of rotation capacity $R_{0.95}$ employed in the present study.

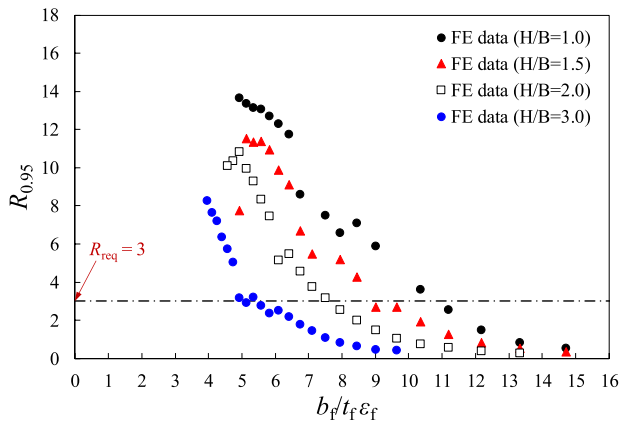
resulting in cross-section aspect ratios ranging from 1.0 to 3.0. The web thickness t_w of each modelled I-section was set to be 0.6 of the corresponding flange thickness t_f (i.e. $t_w = 0.6t_f$), which represents a typical web-to-flange thickness ratio for standard hot-rolled UB and IPE profiles. A total of 20 flange thicknesses t_f , varying from 3.4 mm to 17 mm, was considered for each aspect ratio in order to achieve a broad spectrum of cross-section geometries and flange slendernesses that cover all four classes (i.e. Class 1–4) according to the slenderness limits set out in

prEN 1993–1-1: 2018 [28]. The weld leg length t_{weld} of all the modelled welded I-sections was set equal to 5.6 mm. Three steel grades (S355, S460 and S690) were considered in the parametric studies, allowing the following five combinations of flanges/webs to be studied: (1) homogeneous S690 steel welded I-sections; (2) homogeneous S460 steel welded I-sections; (3) homogeneous S355 steel welded I-sections; (4) hybrid welded I-sections with S690 steel flanges and S460 steel webs; and (5) hybrid welded I-sections with S690 steel flanges and S355 steel webs. The bilinear plus nonlinear hardening material model developed by Yun and Gardner [42] was utilised to represent the full-range stress–strain curves of the S355, S460 and S690 steels. The basic material properties (i.e. E , f_y and f_u) for the S355, S460 and S690 steels used in the parametric studies were taken as the nominal values given in prEN 1993–1-1: 2018 [28], as listed in Table 6, while the full-range stress–strain curves – see Fig. 14, as well as the other key material properties such as ϵ_{li} and ϵ_{sh} , were derived using the predictive model set out in [42]. It should be noted that the structural responses of FE models with predicted stress–strain curves [42], based on measured yield and tensile strengths (see Table 2), and full measured stress–strain curves, were very similar.

The span of each beam model was set at 15 times its outer section height H , and each beam model was loaded in both three-point bending and four-point bending. In order to prevent lateral torsional buckling, uniform and symmetrical lateral restraints were provided along the



(a) Normalised ultimate bending moment (M_u/M_{pl}) versus flange slenderness



(b) Rotation capacity versus flange slenderness

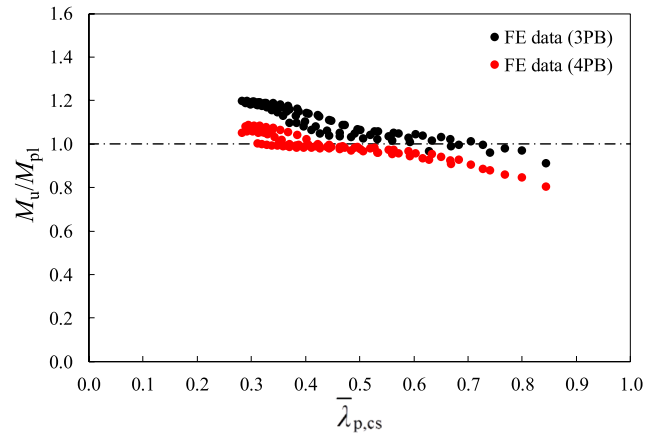
Fig. 18. Influence of cross-section aspect ratio on normalised ultimate bending moment M_u/M_{pl} and rotation capacity $R_{0.95}$ of S690 steel welded I-section beams in three-point bending.

length of the beams at intervals approximately equal to the length that corresponds to a non-dimensional lateral torsional buckling slenderness $\bar{\lambda}_{LT}$ value of 0.2 under pure bending. The lateral restraints were applied at the top and bottom web-to-flange junctions of the sections in order to avoid any influence on the local buckling behaviour of the beam specimens. The ranges of variation of parameters considered in the parametric studies are listed in Table 7, leading to the simulation of a total of 800 welded I-section beams; the generated FE results are presented and analysed in the following section.

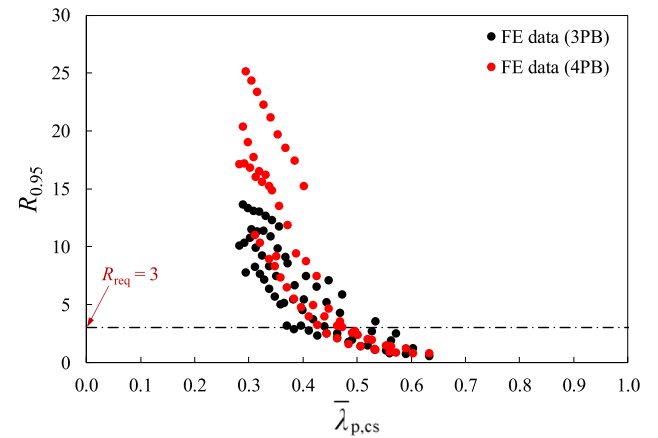
4. Analysis of results and design recommendations for HSS homogeneous welded I-section beams

4.1. General

Current structural steel design standards use the concept of cross-section classification to consider the influence of local buckling on the behaviour and design of cross-sections. Four discrete behavioural classes (i.e. Class 1–4) are typically defined [28]. A Class 1 cross-section can develop its plastic moment capacity M_{pl} in bending and is deemed to have sufficient rotation capacity to allow full redistribution of moments. A Class 2 cross-section is also able to reach its plastic moment capacity M_{pl} but with lower rotation capacity in bending. For a Class 3 cross-section subjected to bending, local buckling occurs after attainment of the elastic moment M_{el} , but before the plastic moment M_{pl} is reached. Hence, the bending resistance of a Class 3 cross-section is limited to its elastic moment capacity M_{el} , or to a linearly interpolated moment



(a) Normalised ultimate bending moment



(b) Rotation capacity

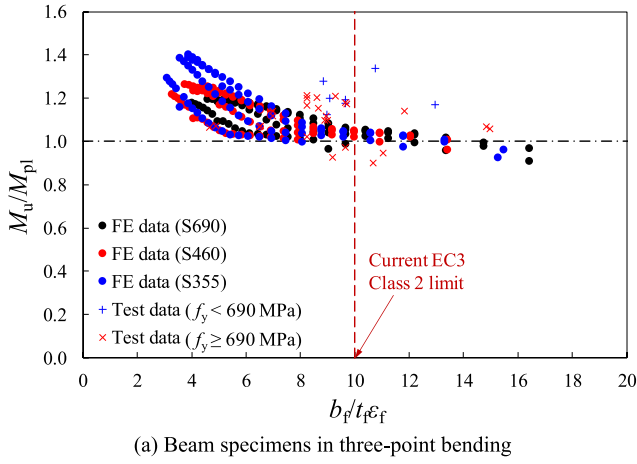
Fig. 19. Influence of moment gradient on normalised ultimate bending moment M_u/M_{pl} and rotation capacity $R_{0.95}$ of S690 steel welded I-section beams.

between M_{el} and M_{pl} [28]. Finally, for a Class 4 cross-section in bending, local buckling occurs prior to the elastic moment being reached; this is accounted for through the effective width method. The classification of a plate element within the cross-section is based on its width-to-thickness ratio (b_f/t_f or h_w/t_w), material (through $\epsilon = (235/f_y)^{0.5}$), boundary conditions and stress distribution. The overall class of a cross-section is defined as the class of the most slender plate element in compression.

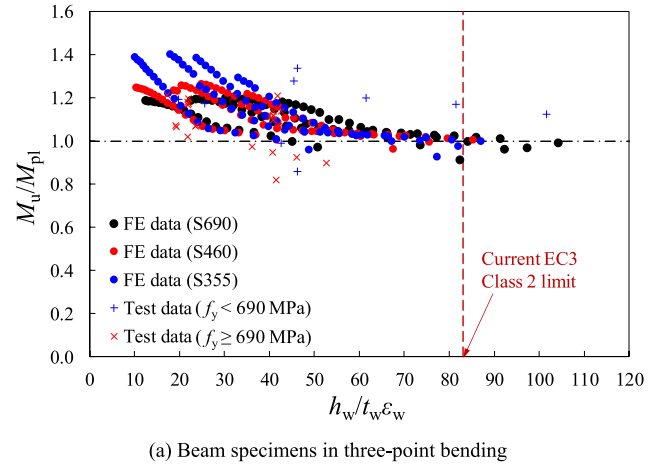
Existing experimental results on HSS welded I-section beams have been collected from the literature and are summarised, along with the test results from the present investigation, in Table 8. These results, together with the numerical data generated from the parametric studies, are used in Sections 4.2 to 4.4 to assess the influence of material grade, cross-section aspect ratio and loading configuration on the ultimate bending resistances and rotation capacities of welded I-section beams subjected to major axis bending. The accuracy of the current cross-section slenderness limits for outstand plate elements in compression and internal plate elements in bending, as specified in Eurocode 3 [14,28], are then evaluated in Section 4.5. Finally, design recommendations for hybrid welded I-section beams are considered in Section 4.6.

4.2. Influence of material grade

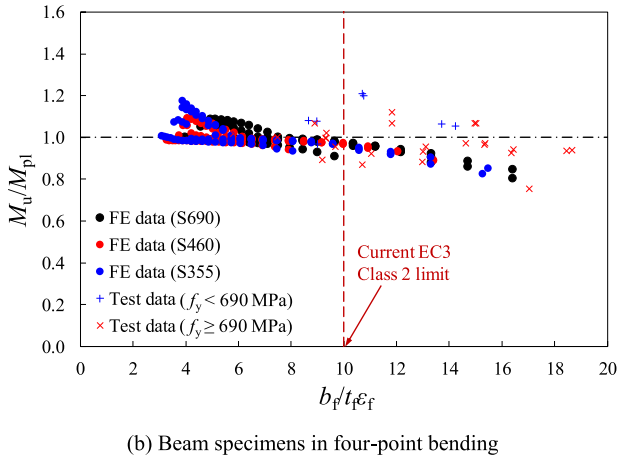
In Fig. 15, the ultimate bending moments M_u obtained from the three-point bending tests and numerical investigations in the three-point



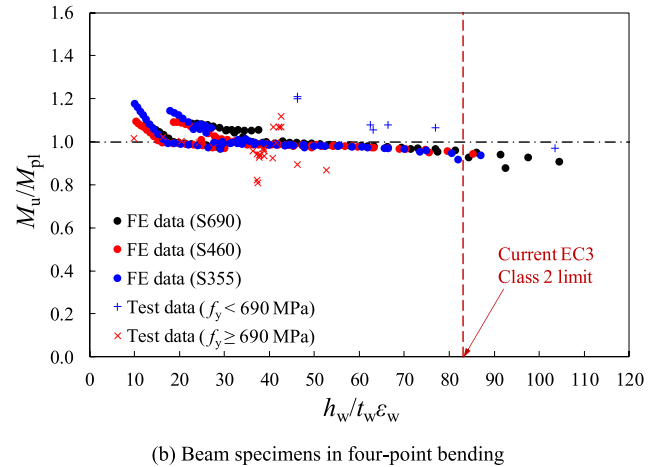
(a) Beam specimens in three-point bending



(a) Beam specimens in three-point bending



(b) Beam specimens in four-point bending



(b) Beam specimens in four-point bending

Fig. 20. Examination of EC3 Class 2 slenderness limit for outstand elements of homogeneous beams in compression.

bending configuration are normalised by the cross-section plastic bending moment M_{pl} , and plotted against the normalised cross-section slenderness $\bar{\lambda}_{p,cs} = (f_y/\sigma_{cr})^{0.5}$, where σ_{cr} is the elastic local buckling stress of the full cross-section, determined using the finite strip software CUFMSM [40]; simplified analytical expressions are also available for determining the elastic local buckling stress of full structural cross-sections [53], considering plate element interaction effects. The normalised ultimate bending moments M_u/M_{pl} of the S690 steel beams and S460 steel beams in three-point bending are compared with those of the S355 steel beams in Fig. 15(a) and (b) respectively. The rotation capacities of the beams are plotted in a similar manner in Fig. 16.

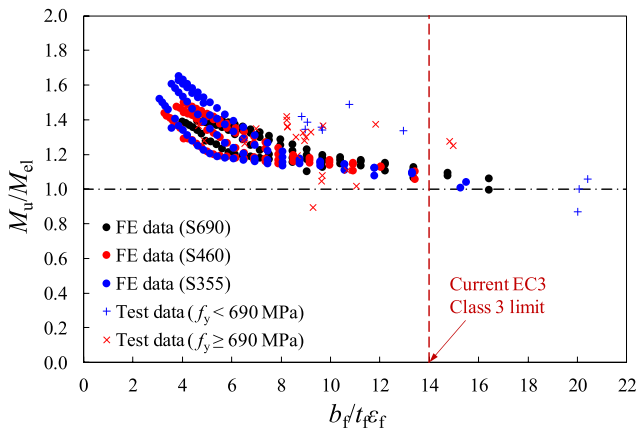
It can be observed from Figs. 15 and 16 that the data points for the HSS steel beams (both S690 and S460 steels) generally follow the same trend as those of the S355 steel beams, especially for beams with slender cross-sections, the failure of which is generally triggered by local buckling at strains below ϵ_{sh} (i.e. strain hardening is not experienced). Slightly lower normalised ultimate bending moment capacities were achieved for the stocky ($\bar{\lambda}_{p,cs} \lesssim 0.35$) S460 steel beams, compared with the corresponding stocky S355 steel beams. The stocky S690 steel beams were able to reach their plastic bending moment M_{pl} , but with the lowest normalised ultimate bending moment capacities. Similarly, the HSS beams exhibited somewhat lower rotation capacities compared with those of the S355 steel beams, as depicted in Fig. 16. The decrease in the normalised ultimate bending moment capacities M_u/M_{pl} and the rotation capacity $R_{0.95}$ (R) for HSS beams with stocky cross-sections relates to their lower level of strain hardening, as indicated in Table 6. Note that throughout this section, rotation capacities have been determined from

Fig. 21. Examination of EC3 Class 2 slenderness limit for internal elements of homogeneous beams in bending.

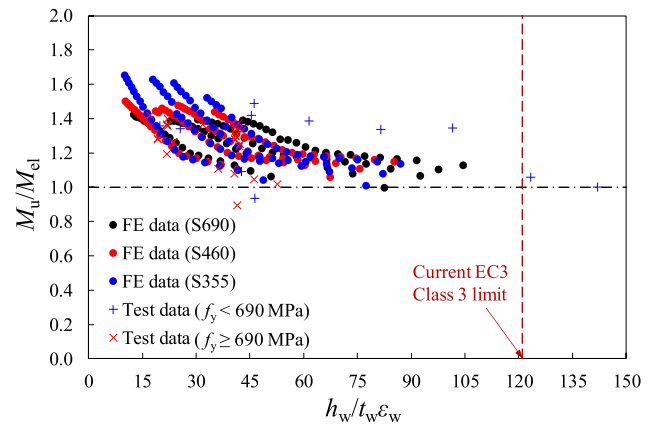
the numerical simulations using a reduced bending moment $0.95M_{pl}$ instead of the plastic bending moment M_{pl} and denoted $R_{0.95}$ (instead of R), as depicted in Fig. 17; the purpose of this is to provide a more stable measure of rotation capacity and avoid anomalies in the results, since the moment-rotation (curvature) curves for stocky beams are typically characterised by a long plateau (particularly in four-point bending) when the cross-section bending moment is in the region of the full plastic bending moment M_{pl} before descending. It is the length of the plateau region that dictates the ability of a cross-section to redistribute moments (rather than the specific value of moment attained), and hence this approach is deemed to be appropriate. The same approach has been employed previously by [16,54–56].

4.3. Influence of cross-section aspect ratio

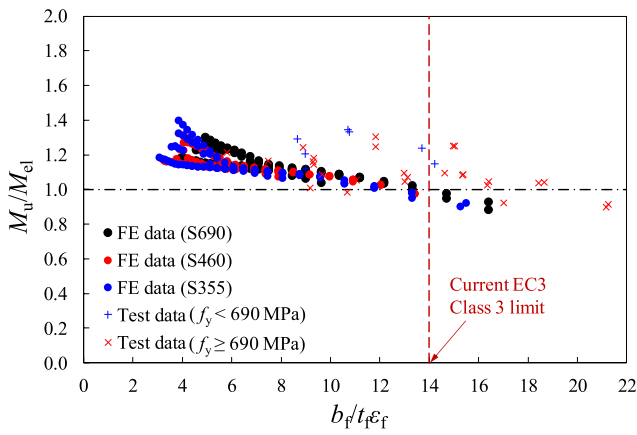
The influence of the cross-section aspect ratio on the normalised ultimate bending moment capacity M_u/M_{pl} and rotation capacity $R_{0.95}$ of S690 steel welded I-sections is discussed in this section. The normalised ultimate bending moments M_u/M_{pl} and rotation capacities $R_{0.95}$ of the S690 steel beams in three-point bending, obtained from the parametric studies, are plotted against the flange slenderness ratio $b_f/t_f\epsilon_f$ in Fig. 18(a) and (b), respectively, where b_f is the outstand width, t_f is the flange thickness and $\epsilon_f = (235/f_{y,f})^{0.5}$, in which $f_{y,f}$ is the yield strength of the flange. The numerically derived data are categorised according to their aspect ratios; the EC3 Class 1 and Class 2 slenderness limits for outstand flanges in compression specified in [14] are also indicated in



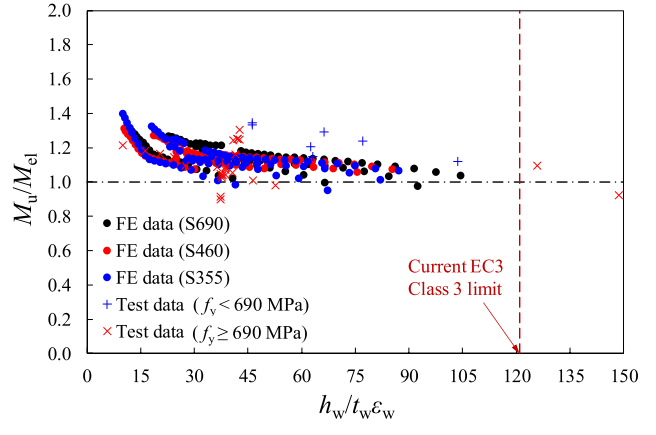
(a) Beam specimens in three-point bending



(a) Beam specimens in three-point bending



(b) Beam specimens in four-point bending



(b) Beam specimens in four-point bending

Fig. 22. Examination of EC3 Class 3 slenderness limit for outstand elements of homogeneous beams in compression.

Fig. 18(a). In addition, the rotation requirement of three ($R_{req} = 3$), which was used in the development of EC3 [16,57,58], is also plotted in Fig. 18(b).

It can be seen from Fig. 18 that lower normalised ultimate bending moment capacities and rotation capacities are achieved for cross-sections with higher aspect ratios for a given flange slenderness; this is caused by the decreasing ability of the web to provide restraint against local buckling to the flange with increasing aspect ratio [53]. This observation echoes the numerical results for the other investigated HSS homogeneous and hybrid welded I-sections, and also mirrors the findings for square and rectangular hollow section (i.e. SHS and RHS) members in bending reported by Wang et al. [17] and Zhou and Long [59].

4.4. Influence of moment gradient

The influence of moment gradient on the flexural behaviour of welded I-sections is examined by comparing the parametric FE results of the S690 steel beams in three-point (3 PB) and four-point (4 PB) bending, with the latter providing the most severe case of uniform bending (i.e. no moment gradient) between the loading points. The normalised ultimate bending moments M_u/M_{pl} and rotation capacities $R_{0.95}$ are plotted against the non-dimensional cross-section slenderness $\bar{\lambda}_{p,cs}$ in Fig. 19(a) and (b), respectively. It can be observed from Fig. 19(a) that for any given cross-section, the beam in three-point bending achieves a higher normalised ultimate bending moment capacity M_u/M_{pl} than that in four-point bending, due to the beneficial effect of the

Fig. 23. Examination of EC3 Class 3 slenderness limit for internal elements of homogeneous beams in bending.

moment gradient. For a beam in three-point bending, the moment gradient within the beam allows the stiffer cross-sections (due to the lower level of plasticity experienced) of the specimen surrounding the mid-span section where the maximum moment arises to delay the development of local buckling. For a beam in four-point bending, on the other hand, the central part between the two loading points where constant moment is applied and experiences essentially the same level of plasticity along the full length, and hence such restraint to delay local buckling is not available. Similar findings were observed for both the homogeneous and hybrid welded I-sections, and have been reported by other researchers on SHS, RHS [17] and elliptical hollow section (EHS) beams [16,60,61]. As shown in Fig. 19(b), the beams with stockier cross-sections in four-point bending generally display higher rotation capacities than their counterparts in three-point bending.

4.5. Assessment of EC3 slenderness limits for the classification of HSS homogeneous welded I-sections

In this subsection, the suitability of the current codified slenderness limits in EN 1993-1-12 (EC3) [14] for the classification of HSS outstand plate elements in compression and HSS internal plate elements in bending is assessed using the experimental results from the literature and the present study, as summarised in Table 8, together with the generated FE results.

4.5.1. Class 2 and Class 3 slenderness limits

To assess the applicability of the current EC3 Class 2 slenderness

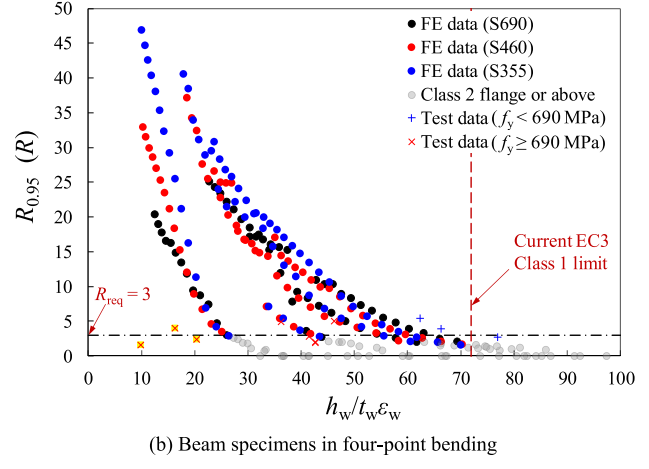
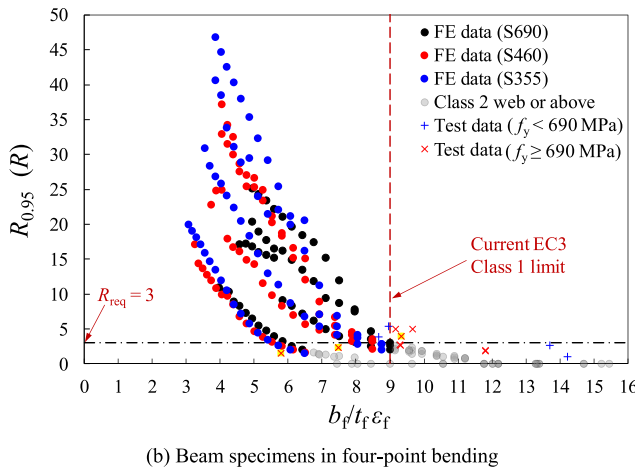
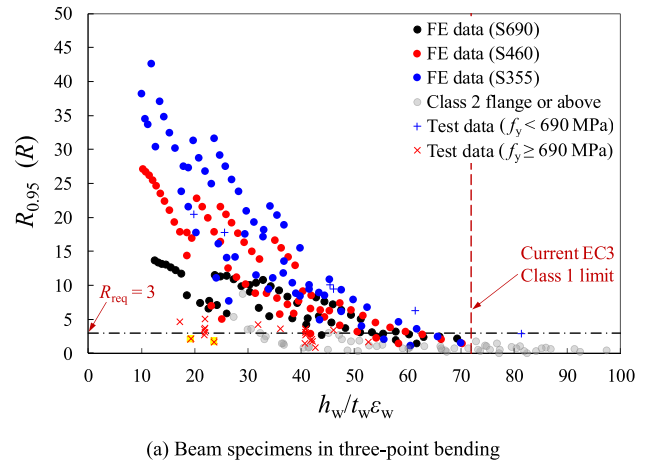
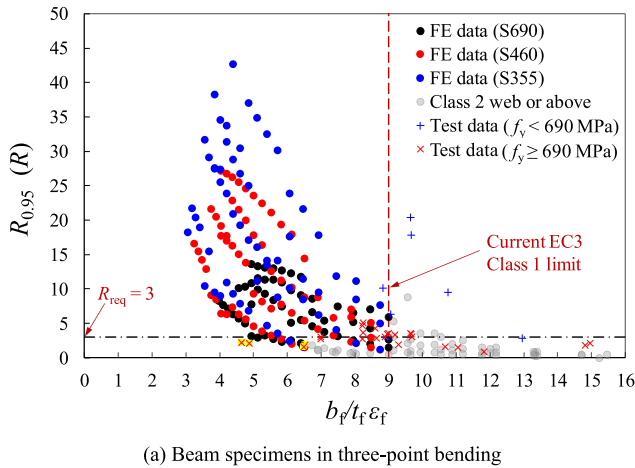


Fig. 24. Examination of EC3 Class 1 slenderness limit for outstand elements in compression in homogeneous welded I-section beams.

Fig. 25. Examination of EC3 Class 1 slenderness limit for internal elements in bending in homogeneous welded I-section beams.

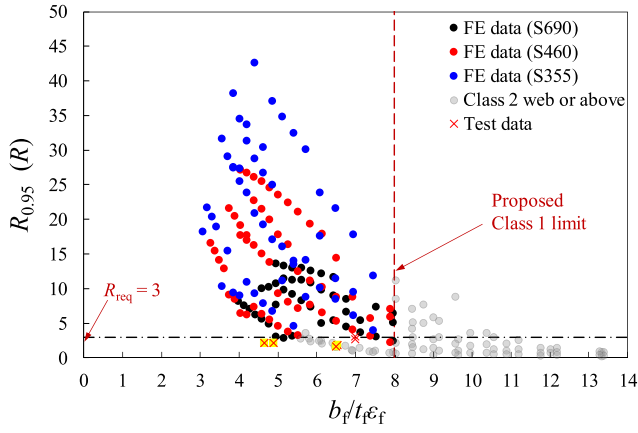
limits for S690 steel outstand elements in compression and internal (i.e. web) elements in bending, the test and numerical ultimate bending moments for the S690 steel welded I-section beams are normalised by the cross-section plastic bending resistances M_{pl} , and plotted against the flange slenderness ($b_f/t_f \epsilon_f$) and web slenderness ($h_w/t_w \epsilon_w$) ratios in Figs. 20 and 21 ((a) for three-point bending and (b) for four-point bending), respectively. The results for the S355 and S460 steel welded I-section beams, together with the current EC3 Class 2 slenderness limits (i.e. $b_f/t_f \epsilon_f = 10$ for outstand elements in compression and $h_w/t_w \epsilon_w = 83$ for internal elements in bending), are also plotted in Figs. 20 and 21 for comparison purposes. It can be seen from Figs. 20 and 21 that the S355, S460 and S690 data points generally follow the same trend, and the current EC3 Class 2 slenderness limits are therefore deemed suitable for the classification of S690 steel welded I-section beams. It should be noted though, that for all steel grades, the data points for the cross-sections that are within the slenderness limits often fall below M_{pl} in the case of four-point bending; as discussed in Section 4.4, this is related to the reduced restraint against local buckling afforded to the critical cross-section in the case of uniform bending (compared to three-point bending) and hence the reduced ability to benefit from strain hardening to enable capacities beyond M_{pl} to be achieved.

The current EC3 Class 3 slenderness limits for S690 steel outstand elements in compression and internal (i.e. web) elements in bending are also assessed in Figs. 22 and 23, respectively, where the test and numerical ultimate bending moments are now normalised by the cross-section elastic bending resistances M_{el} . The comparisons shown in Figs. 22 and 23 confirm the suitability of the current EC3 Class 3

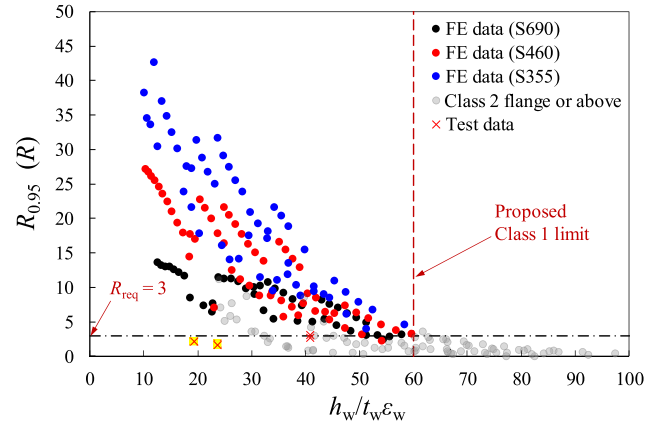
slenderness limits for S690 steel welded I-sections subjected to major axis bending.

4.5.2. Class 1 slenderness limits

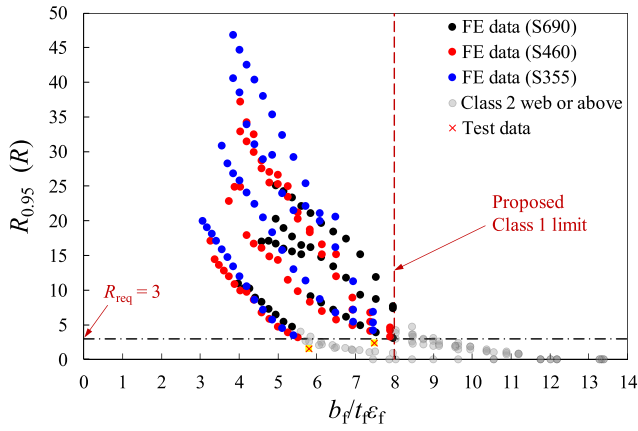
To assess the current EC3 Class 1 slenderness limits, the rotation capacities from both the experiments (R) and FE models ($R_{0.95}$) are plotted against the flange slenderness ($b_f/t_f \epsilon_f$) and web slenderness ($h_w/t_w \epsilon_w$) ratios in Figs. 24 and 25 respectively, together with the current EC3 Class 1 slenderness limits (i.e. $b_f/t_f \epsilon_f = 9$ for outstand elements in compression and $h_w/t_w \epsilon_w = 72$ for internal elements in bending) and the rotation capacity requirement of $R_{req} = 3$ for Class 1 cross-sections. Note that the use of R (instead of $R_{0.95}$) was retained for the experiments since rotation capacities were typically reported in the literature using this measure. It can be seen from Figs. 24 and 25 that the current EC3 Class 1 slenderness limits appear somewhat unconservative for both NSS and HSS welded I-sections. Note that when the outstand flange slenderness limits are being assessed (i.e. in Fig. 24), the data points corresponding to the cross-sections where the web is Class 2 or above are shaded in grey, since both the flange and web must be Class 1 for plastic design to be applied. The same approach is used when assessing the web slenderness limits in Fig. 25. Lower slenderness limits of $b_f/t_f \epsilon_f = 8$ for outstand elements in compression and $h_w/t_w \epsilon_w = 60$ for internal plate elements in bending are thus proposed to provide improved predictions of when $R_{req} = 3$ can be achieved for both NSS and HSS welded I-sections. The slightly stricter proposed slenderness limits are considered to be essential for HSS due to the lack of historical precedent in applying plastic design to HSS structures. The rotation capacities of the newly



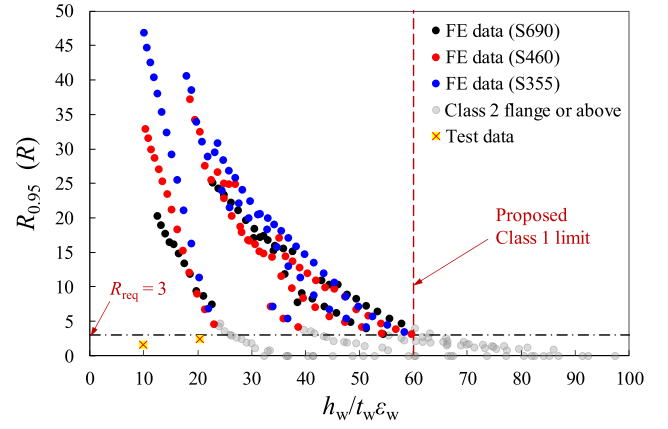
(a) Beam specimens in three-point bending



(a) Beam specimens in three-point bending



(b) Beam specimens in four-point bending



(b) Beam specimens in four-point bending

Fig. 26. Examination of the proposed Class 1 slenderness limit for outstand elements in compression in homogeneous welded I-section beams.

classified Class 1 cross-sections are plotted against their flange and web slenderness ratios in Figs. 26 and 27, together with the proposed Class 1 slenderness limits for outstand flanges (in compression) and internal elements (in bending), which provide predictions of when $R_{req} = 3$ can be achieved. Note that the data points shaded in yellow indicate tests carried out in the present study that were terminated prior to reaching the full rotation capacity R .

4.6. Analysis of results and design recommendations for HSS hybrid welded I-section beams

In this section, the structural performance of HSS hybrid welded I-section beams subjected to major axis bending is discussed and the applicability of the EC3 design rules to these sections is evaluated based on the established test and FE results.

4.6.1. Bending resistance

The elastic bending moment M_{el} of the investigated HSS hybrid welded I-sections in major axis bending is defined herein as the bending moment at which the stress at the extreme outer-fibre of the flanges reaches the material yield strength $f_{y,f}$ (i.e. the strain at the extreme outer-fibre of the flanges reaches the yield strain of the flange plates $\epsilon_{y,f}$). The strain and stress distributions throughout the depth of an HSS hybrid welded I-section at the defined elastic bending moment M_{el} are shown in Fig. 28, assuming a linear elastic strain distribution and elastic-perfectly-plastic material behaviour for both the flanges and the web. From the presented stress distribution, M_{el} can be determined from:

Fig. 27. Examination of the proposed Class 1 slenderness limit for internal elements in bending in homogeneous welded I-section beams.

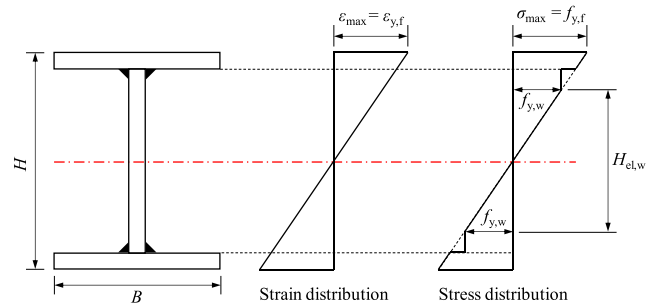


Fig. 28. Strain and stress distributions for an HSS hybrid welded I-section in major axis bending at the defined elastic bending moment M_{el} .

$$M_{el} = W_{el,f} f_{y,f} + W_{el,w} f_{y,w} + W_{pl,w} f_{y,w} \quad (7)$$

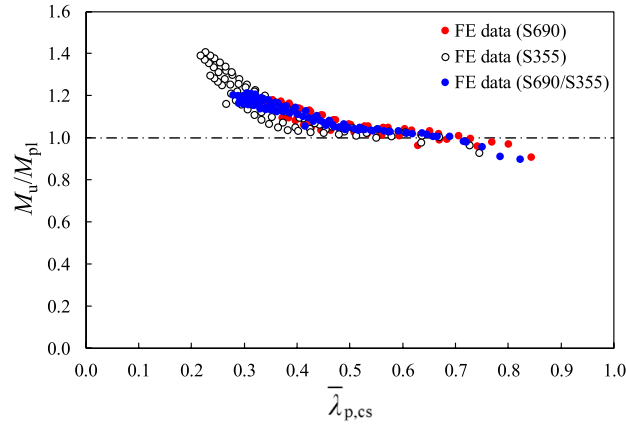
where $W_{el,f}$ and $W_{el,w}$ are the elastic section moduli associated with the flanges and the elastic portion of the web, respectively, as given by:

$$W_{el,f} = \frac{B t_f^3 / 3 + B t_f (H - t_f)^2}{H} \quad (8)$$

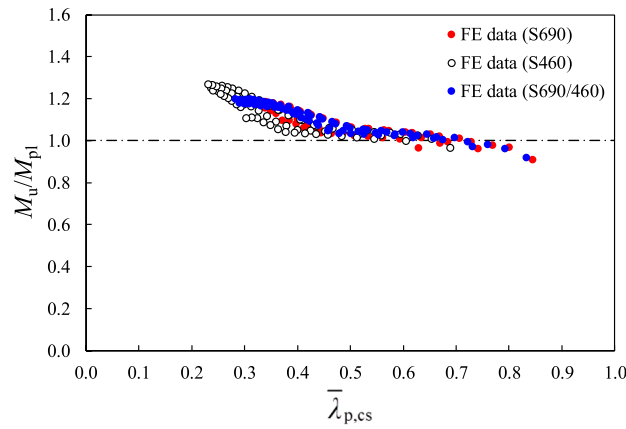
and

$$W_{el,w} = \frac{1}{6} t_w H_{el,w}^2 \quad (9)$$

$W_{pl,w}$ is the plastic section modulus associated with the plastic



(a) Hybrid beams (composed of S690 steel flanges and an S355 steel web) and S355 steel and S690 steel homogeneous beams



(b) Hybrid beams (composed of S690 steel flanges and an S460 steel web) and S460 steel and S690 steel homogeneous beams

Fig. 29. Comparison of normalised ultimate bending resistances M_u/M_{pl} for homogeneous and hybrid welded I-section beams under three-point bending.

portion of the web, as given by:

$$W_{pl,w} = 2t_w \cdot \left(\frac{H}{2} - \frac{H_{el,w}}{2} - t_f \right) \cdot \left(t_f - \frac{H}{2} + H_{el,w} \right) \quad (10)$$

$f_{y,f}$ and $f_{y,w}$ are the yield strengths of the flange and the web plates, respectively, and $H_{el,w}$ is the height of the elastic portion of the web, as illustrated in Fig. 28 and given by:

$$H_{el,w} = \frac{f_{y,w}/E_w}{f_{y,f}/E_f} H \quad (11)$$

where E_f is the Young's modulus of the flange plate and E_w is the Young's modulus of the web plate.

Similar to homogeneous welded I-sections, the plastic bending moment M_{pl} for the investigated HSS hybrid welded I-sections in major axis bending is defined as the moment at which the cross-section is fully yielded, i.e. the flange plates and the web plate are at their corresponding yield strengths.

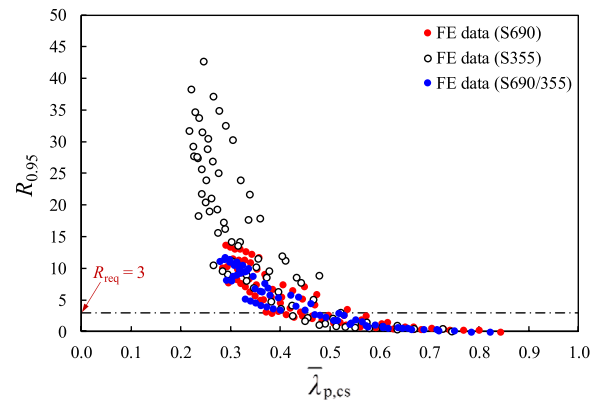
The normalised ultimate bending resistances M_u/M_{pl} are plotted against the non-dimensional cross-section slenderness $\bar{\lambda}_{p,cs}$ in Fig. 29(a) for the hybrid beams composed of S690 steel flanges and an S355 steel web, as well as the S355 steel and S690 steel homogeneous beams, in three-point bending. The equivalent graph for the hybrid beams composed of S690 steel flanges and an S460 steel web, as well as the S460 steel and S690 steel homogeneous beams in three-point bending is shown in Fig. 29(b). Note that the non-dimensional cross-section slenderness $\bar{\lambda}_{p,cs}$ for hybrid beams is defined by Eq. (12):

$$\bar{\lambda}_{p,cs} = \sqrt{\frac{M_{el}}{M_{cr}}} = \sqrt{\frac{M_{el}}{\sigma_{cr} W_{el}}} \quad (12)$$

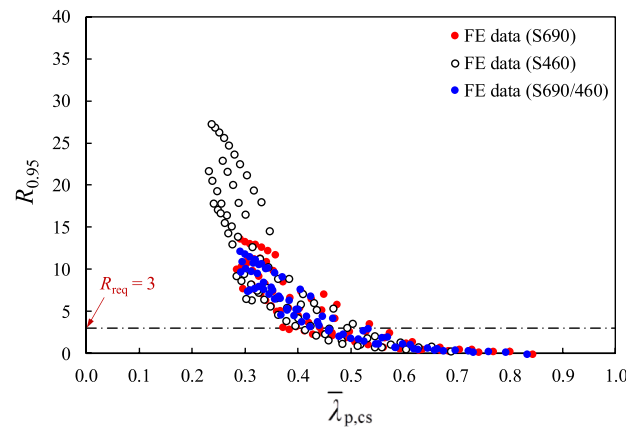
where M_{el} is the elastic bending moment calculated from Eqs. (7)-(11), σ_{cr} is the elastic local buckling stress of the full cross-section determined using the finite strip software CUFSM [40] and W_{el} is cross-sectional elastic section modulus. It can be observed from Fig. 29 that the data points for the hybrid beams generally follow a similar trend to that of the homogeneous beams, especially for the beams with more slender cross-sections, for which failure occurred prior to the maximum strain within the critical region of the beam specimens reaching the strain hardening strain ϵ_{sh} . For the beams with stockier cross-sections, where capacity benefits are derived from strain hardening, the normalised ultimate bending resistances M_u/M_{pl} for the hybrid beams are more similar to those of the homogeneous beams made of the higher steel grade (i.e. the steel grade of the flange plates of the hybrid beams), since the strain hardening contribution is largely dependent on the material characteristics of the flange plates.

4.6.2. Rotation capacity

The rotation capacities of the investigated homogeneous and hybrid beams under three-point bending are plotted against the non-dimensional slenderness $\bar{\lambda}_{p,cs}$ in Fig. 30. Similar to the behaviour observed for the normalised bending resistances, the rotation capacities of the HSS hybrid beams generally follow the same trend as that of the homogeneous beams, especially for the beams with the more slender



(a) Hybrid beams (composed of S690 steel flanges and an S355 steel web) and S355 steel and S690 steel homogeneous beams



(b) Hybrid beams (composed of S690 steel flanges and an S460 steel web) and S460 steel and S690 steel homogeneous beams

Fig. 30. Comparison of rotation capacities $R_{0.95}$ for homogeneous and hybrid welded I-section beams in three-point bending.

cross-sections. The hybrid beams with the stockier cross-sections (i.e. with $\bar{\lambda}_{p,cs}$ lower than about 0.4) exhibit lower rotation capacities compared with their homogeneous counterparts made of the lower steel grade (i.e. S355 or S460 steel). Compared to the HSS homogeneous beams, the HSS hybrid beams subjected to the major axis bending experience gradual plastification of the web (i.e. initiating from the outer-fibre of the web plate) prior to the yielding of the flanges, which reduces the ability of the web to provide rotational restraint to the flanges against local buckling. The rotation capacities of the HSS hybrid beams are thus also somewhat lower than those of the counterpart homogeneous beams made of the higher steel grade; this is more pronounced for the hybrid beams that have a higher yield strength ratio of $f_{y,f}/f_{y,w}$, as seen in Fig. 30(a). It is recommended that for HSS hybrid welded I-sections, the yield strength of the flange plates should be no higher than twice the yield strength of the web (i.e. $f_{y,f} \leq 2f_{y,w}$) [41], since hybrid girders with greater ratios of $f_{y,f}/f_{y,w}$ show significantly reduced rotation capacities.

4.6.3. Assessment of EC3 slenderness limits for the classification of HSS hybrid welded I-sections

The test and numerical ultimate bending moments of the hybrid welded I-section beams M_u are normalised by the cross-section elastic bending moment capacities M_{el} (calculated according to Eqs. (7)–(11)), and plotted against the flange slenderness ($b_f/t_f \epsilon_f$) and web slenderness ($h_w/t_w \epsilon_w$) ratios in Figs. 31 and 32 respectively. The Class 3 slenderness limits for outstand flanges in compression and internal webs in bending set out in EN 1993–1–12 [14] are also plotted in Figs. 31 and 32 respectively. The comparisons show that the current EC3 Class 3 slenderness limits for HSS welded I-

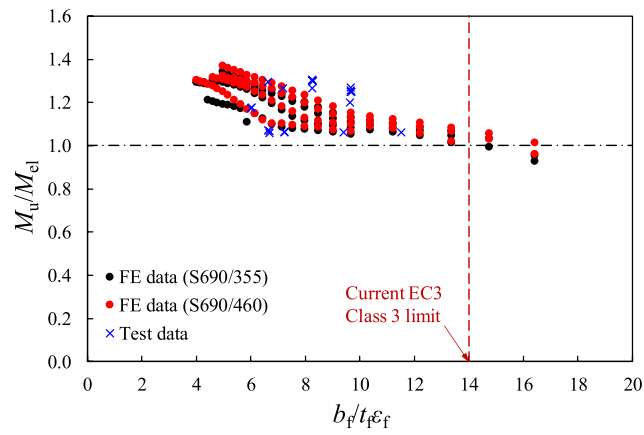
sections are also applicable to HSS hybrid welded I-sections.

Similarly, the current EC3 Class 2 slenderness limits set out in EN 1993–1–12 [14] are examined in Figs. 33 and 34, where the test and numerical ultimate bending moments M_u for the HSS hybrid beams in major axis bending are now normalised by the cross-section plastic bending moments M_{pl} . Again, the comparisons confirm the suitability of the current EC3 Class 2 slenderness limits for HSS hybrid welded I-sections in major axis bending.

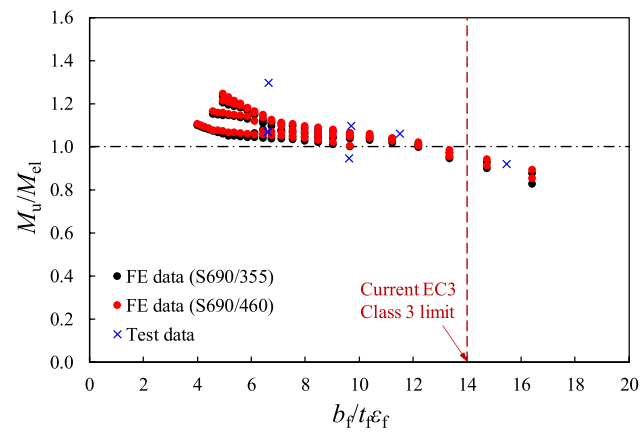
Finally, the rotation capacities from the experiments (R) and FE models ($R_{0.95}$) of the HSS hybrid beams are plotted against the flange slenderness ratio $b_f/t_f \epsilon_f$ in Fig. 35 and the web slenderness ratio $h_w/t_w \epsilon_w$ in Fig. 36. The proposed more strict Class 1 slenderness limits for HSS homogeneous welded I-section beams are also plotted in Figs. 35 and 36. The comparisons reveal that the proposed Class 1 slenderness limits are also suitable for the classification of HSS hybrid welded I-section beams in major axis bending.

5. Conclusions

Testing, finite element modelling and design aspects of high strength steel (HSS) beams have been described in this paper. An experimental programme, which included a total of six in-plane major axis three-point bending tests on both HSS homogeneous and hybrid welded I-sections, was carried out. The test setup, including the use of a bespoke restraint system to prevent lateral torsional buckling and the employment of DIC to monitor the strain histories of the most heavily loaded regions of the beam specimens, as well as the test results have been carefully presented and analysed. The test results obtained from the present study, as well as those

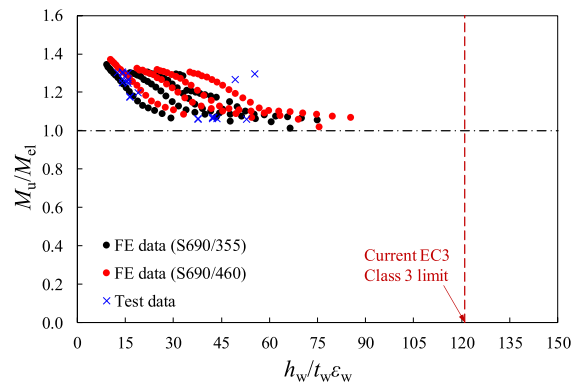


(a) Beam specimens in three-point bending

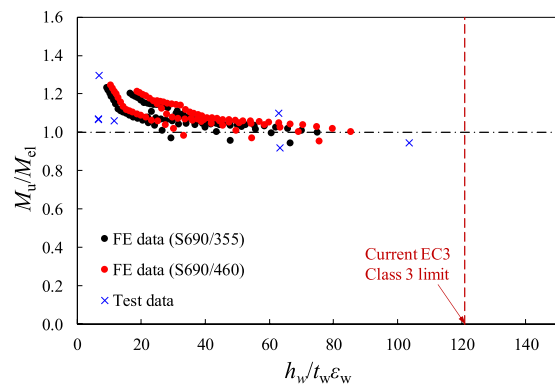


(b) Beam specimens in four-point bending

Fig. 31. Examination of EC3 Class 3 slenderness limit for outstand flanges in compression in HSS hybrid beams.

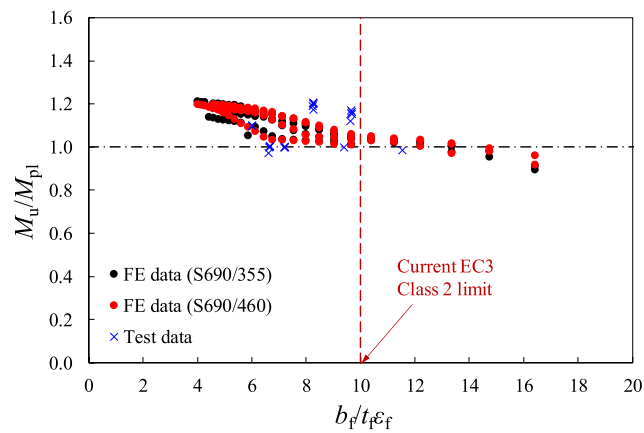


(a) Beam specimens in three-point bending

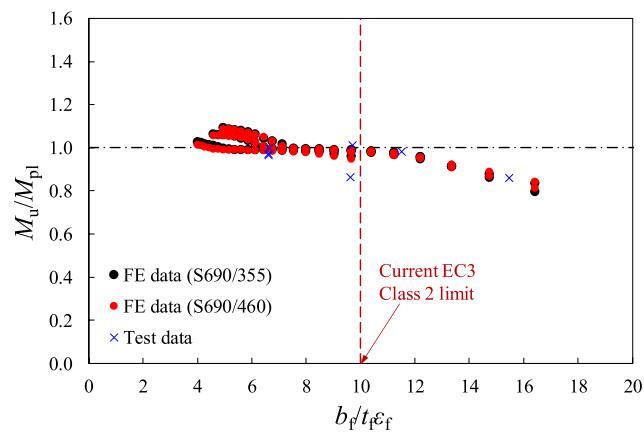


(b) Beam specimens in four-point bending

Fig. 32. Examination of EC3 Class 3 slenderness limit for internal plate elements in bending in HSS hybrid beams.

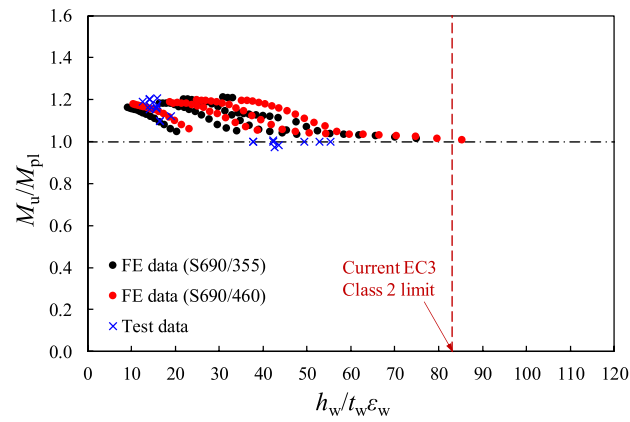


(a) Beam specimens in three-point bending

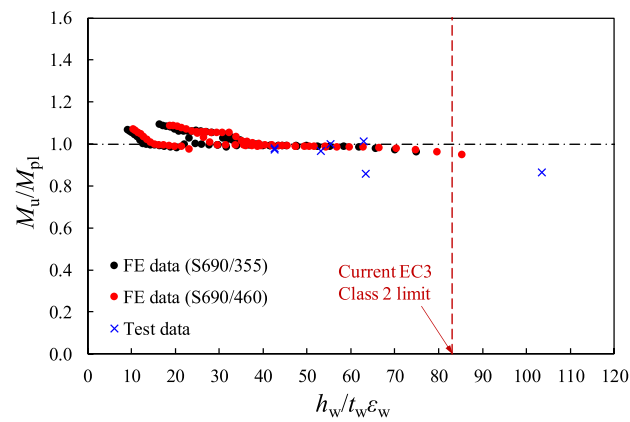


(b) Beam specimens in four-point bending

Fig. 33. Examination of EC3 Class 2 slenderness limit for outstand flanges in compression in HSS hybrid beams.

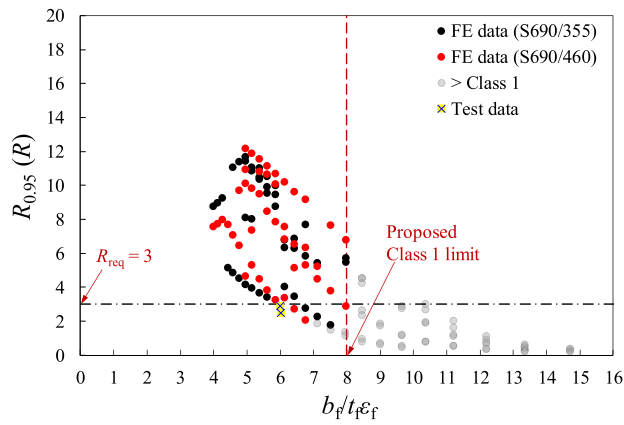


(a) Beam specimens in three-point bending

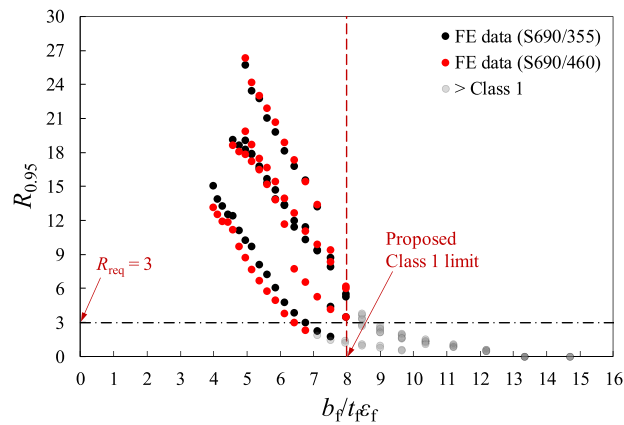


(b) Beam specimens in four-point bending

Fig. 34. Examination of EC3 Class 2 slenderness limit for internal plate elements in compression in HSS hybrid beams.



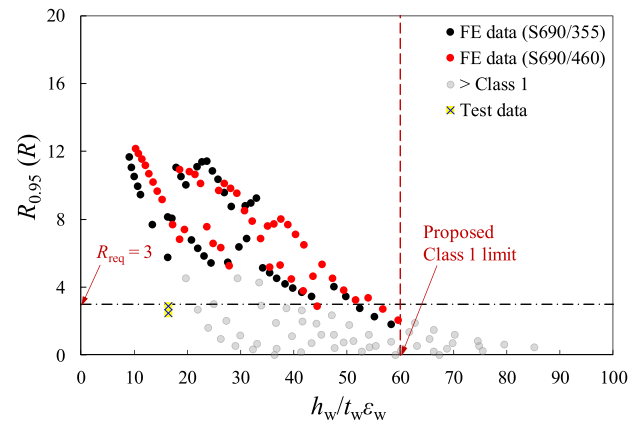
(a) Beam specimens in three-point bending



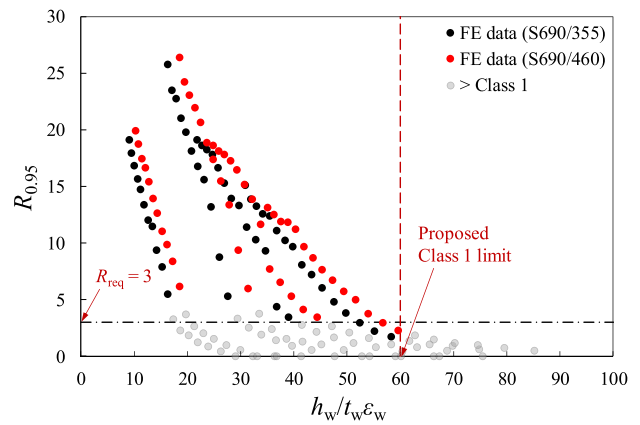
(b) Beam specimens in four-point bending

Fig. 35. Examination of the proposed Class 1 slenderness limit for outstand flanges in compression in HSS hybrid beams.

collected from the literature, were subsequently employed in a parallel numerical modelling programme for the validation of FE models. An extensive parametric study was then carried out to generate additional structural performance data for the assessment of the influence of the material grade, cross-section aspect ratio and moment gradient on the flexural behaviour of HSS welded I-sections. The obtained test and FE results were also used to evaluate the applicability of the current EC3 cross-section classification limits [14] to both HSS homogeneous and hybrid welded I-sections subjected to major axis bending. It was confirmed that the current EC3 Class 2 and 3 slenderness limits are suitable to classify the outstand flanges (in compression) and internal webs (in bending) of both HSS homogeneous and hybrid welded I-sections. To satisfy the rotation capacity requirement of 3, stricter Class 1 slenderness limits for outstand flanges in compression (i.e. $b_f/t_f \epsilon_f = 8$) and internal webs in bending ($h_w/t_w \epsilon_w = 60$) were proposed; the use of the new limits is considered to be essential to allow the plastic design of HSS homogeneous and hybrid systems. Although the present study is focussed on the behaviour and design of HSS welded I-section beams subjected to in-plane major axis bending, research has been carried out on HSS welded I-section beams susceptible to lateral torsional buckling [20,21,62–64] and subjected to minor axis bending [13], leading to improved design rules. It should be noted that the present study is limited to structural behaviour and design of HSS beams made of non-slender welded I-sections; there remains scope for further research on HSS beams made of slender welded I-sections and on the development of the deformation based approach [65] to both HSS and hybrid I-section members.



(a) Beam specimens in three-point bending



(b) Beam specimens in four-point bending

Fig. 36. Examination of the proposed Class 1 slenderness limit for internal plate elements in bending in HSS hybrid beams.

Declaration of Competing Interest

The authors declare that they have no known competing financial interests or personal relationships that could have appeared to influence the work reported in this paper.

Data availability

Data will be made available on request.

Acknowledgements

This project has received funding from the Research Fund for Coal and Steel under grant agreement no. 743504. The authors would also like to thank Mr. Les Clark for his assistance and advice during the execution of this project.

References

- [1] Bjorhovde R. Development and use of high performance steel. *J Constr Steel Res* 2004;60:393–400.
- [2] Miki C, Homma K, Tominaga T. High strength and high performance steels and their use in bridge structures. *J Constr Steel Res* 2002;58:3–20.
- [3] Graham P. High strength steel use in Australia. *Japan and the US Struct Eng* 2006; 11:27–30.
- [4] Ban HY, Shi G, Shi YQ, Wang YJ. Overall buckling behavior of 460MPa high strength steel columns: Experimental investigation and design method. *J Constr Steel Res* 2012;74:140–50.
- [5] Shi G, Ban HY, Bijlaard FSK. Tests and numerical study of ultra-high strength steel columns with end restraints. *J Constr Steel Res* 2012;70:236–47.

- [6] Kim DK, Lee CH, Han KH, Kim JH, Lee SE, Sim HB. Strength and residual stress evaluation of stub columns fabricated from 800MPa high-strength steel. *J Constr Steel Res* 2014;102:111–20.
- [7] Shi G, Zhou WJ, Bai Y, Lin CC. Local buckling of 460MPa high strength steel welded section stub columns under axial compression. *J Constr Steel Res* 2014;100:60–70.
- [8] Ban HY, Shi G, Shi YJ, Bradford MA. Experimental investigation of the overall buckling behaviour of 960MPa high strength steel columns. *J Constr Steel Res* 2013;88:256–66.
- [9] Tse K, Wang J, Yun X. Structural behaviour and continuous strength method design of high strength steel non-slender welded I-section beam-columns. *Thin-Walled Struct* 2021;169:108273.
- [10] Ma TY, Hu YF, Liu X, Li GQ, Chung KF. Experimental investigation into high strength Q690 steel welded H-sections under combined compression and bending. *J Constr Steel Res* 2017;138:449–62.
- [11] McDermott JF. Plastic bending of A514 steel beams. *J Struct Div* 1969;95(9):1851–71.
- [12] Beg D, Hladnik L. Slenderness limit of class 3 I cross-sections made of high strength steel. *J Constr Steel Res* 1996;38(3):201–17.
- [13] Sun Y, He A, Liang YT, Zhao O. In-plane bending behaviour and capacities of S690 high strength steel welded I-section beams. *J Constr Steel Res* 2019;162:105741.
- [14] EN 1993-1-12:2007. Eurocode 3: Design of steel structures – Part 1-12: Additional rules for the extension of EN 1993 up to steel grades S700. European Committee for Standardization (CEN), Brussels; 2007.
- [15] Bartsch H, Eyben F, Pauli G, Schaffrath S, Feldmann M. Experimental and numerical investigations on the rotation capacity of high-strength steel beams. *J Struct Eng* 2021;147(6):04021067.
- [16] Chan TM, Gardner L. Bending strength of hot-rolled elliptical hollow sections. *J Constr Steel Res* 2008;64:971–86.
- [17] Wang J, Afshan S, Gkantou M, Theofanous M, Baniotopoulos C, Gardner L. Flexural behaviour of hot-finished high strength steel square and rectangular hollow sections. *J Constr Steel Res* 2016;121:97–109.
- [18] Meng X, Gardner L. Cross-sectional behaviour of cold-formed high strength steel circular hollow sections. *Thin-Walled Struct* 2020;156:106822.
- [19] Suzuki T, Ogawa T, Ikarashi K. A study on local buckling behavior of hybrid beams. *Thin-Wall Struct* 1994;19(2–4):337–51.
- [20] Shokouhian M, Shi Y. Flexural strength of hybrid steel I-beams based on slenderness. *Eng Struct* 2015;93:114–28.
- [21] Shokouhian M, Shi Y. Investigation of ductility in hybrid and high strength steel beams. *Int J Steel Struct* 2014;14(2):265–79.
- [22] GB 50017-2003. Code for design of steel structures. Ministry of Construction of the People's Republic of China, China Architecture and Building Press, Beijing; 2003.
- [23] EN 1993-1-1:2005. Eurocode 3: Design of steel structures – Part 1-1: General rules and rules for buildings. European Committee for Standardization (CEN), Brussels; 2005.
- [24] ANSI/AISC 360-16. Specification for Structural Steel Buildings, American Institute of Steel Construction (AISC), Chicago, Illinois, 2016.
- [25] EN. 10025–2. Hot rolled products of structural steels – Part 1: Technical delivery conditions for non-alloy structural steels. Brussels: European Committee for Standardization (CEN); 2004.
- [26] EN. 10025–6. Hot rolled products of structural steels – Part 1: Technical delivery conditions for flat products of high yield strength structural steels in the quenched and tempered condition. Brussels: European Committee for Standardization (CEN); 2004.
- [27] EN ISO. 6892–1. Metallic Materials: Tensile Testing – Part 1: Method of test at room temperature. Brussels: European Committee for Standardization (CEN); 2016.
- [28] prEN 1993-1-1:2018. Eurocode 3: Design of steel structures – Part 1-1: General rules and rules for buildings. European Committee for Standardization (CEN), Brussels; 2018. Final document.
- [29] Yun X, Zhu YF, Wang ZX, Gardner L. Benchmark tests on high strength steel I-section frames. *Eng Struct* 2022;258:114108.
- [30] DaVis. Product-Manual Davis 8.4. LaVision [Software] 2017.
- [31] Abaqus 2018. SIMULIA - Dassault Systèmes; 2018.
- [32] Yun X, Gardner L, Boissonnade N. Ultimate capacity of I-sections under combined loading – Part 1: Experiments and FE model validation. *J Constr Steel Res* 2018;147:408–21.
- [33] Bu Y, Gardner L. Local stability of laser-welded stainless steel I-sections in bending. *J Constr Steel Res* 2018;148:49–64.
- [34] Bu Y, Gardner L. Finite element modelling and design of welded stainless steel I-section columns. *J Constr Steel Res* 2019;152:57–67.
- [35] Tankova T, Simões da Silva L, Balakrishnam M, Rodrigues D, Launert B, Pasternak H, et al. Residual stresses in welded I section steel members. *Eng Struct* 2019;197:109398.
- [36] Liu X, Chung KF. Experimental and numerical investigation into temperature histories and residual stress distributions of high strength steel S690 welded H-sections. *Eng Struct* 2018;165:396–411.
- [37] Li TJ, Li GQ, Wang YB. Residual stress tests of welded Q690 high-strength steel box- and H-sections. *J Constr Steel Res* 2015;115:283–9.
- [38] Yun X, Zhu YF, Meng X, Gardner L. Normal and high strength steel welded I-section columns: Residual stress distributions, testing, simulation and design. *Eng Struct* (submitted).
- [39] Fieber A, Gardner L, Macorini L. Formulae for determining elastic local buckling half-wavelengths of structural steel cross-sections. *J Constr Steel Res* 2019;159:493–506.
- [40] Schafer B, Ádány S. Buckling analysis of cold-formed steel members using CUFSM: conventional and constrained finite strip methods. Proceedings of the 18th International Specialty Conference on Cold-Formed Steel Structures, Orlando, FL, USA; 2006:39-54.
- [41] EN 1993-1-5:2006. Eurocode 3: Design of steel structures – Part 1-5: Plated structural elements. European Committee for Standardization (CEN), Brussels; 2006.
- [42] Yun X, Gardner L. Stress-strain curves for hot-rolled steels. *J Constr Steel Res* 2017;133:36–46.
- [43] Lee CH, Han KH, Uang CM, Kim DK, Park CH, Kim JH. Flexural strength and rotation capacity of I-shaped beams fabricated from 800-MPa steel. *J Struct Eng* 2013;139:1043–58.
- [44] Schillo N, Feldmann M. Experiments on the rotational capacity of beams made of high-strength steel. *Steel Constr* 2018;11:42–8.
- [45] Shi YJ, Xu KL. Experimental and analytical study on local buckling behavior of high strength steel welded I-section beams. *Int J Steel Struct* 2019;19:1171–90.
- [46] Shi YJ, Xu KL, Shi G, Li YX. Local buckling behavior of high strength steel welded I-section flexural members under uniform moment. *Adv Struct Eng* 2018;21:93–108.
- [47] Wang CS, Duan L, Chen YF, Wang SC. Flexural behavior and ductility of hybrid high performance steel I-girders. *J Constr Steel Res* 2016;125:1–14.
- [48] GB/T 1591–2008. High Strength Low Alloy Structural Steels. Ministry of Construction of the People's Republic of China. Beijing: China Architecture and Building Press; 2008.
- [49] JIS G 3106:1999. Rolled steels for welded structure. Japanese Standards Association (JIS). 2002.
- [50] GB/T 16270–2009. High strength structural steel plates in the quenched and tempered condition. Ministry of Construction of the People's Republic of China. Beijing: China Architecture and Building Press; 2009.
- [51] ASTM A709/A709M-18. Standard Specification for Structural Steel for Bridges. ASTM International; 2018.
- [52] GB/T 700–2006. Carbon structural steels. Ministry of Construction of the People's Republic of China. Beijing: China Architecture and Building Press; 2006.
- [53] Gardner L, Fieber A, Macorini L. Formulae for calculating elastic local buckling stresses of full structural cross-sections. *Structures* 2019;17:2–20.
- [54] Lay MG, Galambos TV. Inelastic steel beams under uniform moment. *J Struct Div* 1965;91(6):67–93.
- [55] Bartsch H, Eyben F, Schaffrath S, Feldmann M. On the plastic design of high-strength steel beams. *Steel Constr* 2021;14:222–35.
- [56] Sedlacek G, Dahl W, Stranghöner N, Kalinowski B, Rondal J, Boeraeve P. Investigation of the rotation behaviour of hollow section beams. ECSC Research project, final report, 7210/SA/119; 1995.
- [57] Bild S, Roik K, Sedlacek G, Stutzki Ch, Spangemacher R. Background document for chapter 5 of Eurocode 3 – The b/t-ratios controlling the applicability of analysis models in Eurocode 3. Draft Aachen 1989.
- [58] Sedlacek G, Feldmann M. Background document 5.09 for chapter 5 of Eurocode 3 Part 1.1 – The b/t ratios controlling the applicability of analysis models in Eurocode 3 Part 1.1. Aachen. 1995.
- [59] Zhou F, Long G. Element interaction of cold-formed stainless steel cross-sections subjected to major axis bending. *J Constr Steel Res* 2016;118:22–40.
- [60] Chen M-T, Young B. Behavior of cold-formed steel elliptical hollow sections subjected to bending. *J Constr Steel Res* 2019;158:317–30.
- [61] Chen M-T, Young B. Structural behavior of cold-formed steel semi-oval hollow section beams. *Eng Struct* 2019;185:400–11.
- [62] Tankova T, Rodrigues F, Leitão C, Martins C, Simões da Silva L. Lateral-torsional buckling of high strength steel beams: Experimental resistance. *Thin-Walled Struct* 2021;164:107913.
- [63] Tankova T, Simões da Silva L, Rodrigues F. Buckling curve selection for HSS welded I-section members. *Thin-Walled Struct* 2022;177:109430.
- [64] Le T, Bradford MA, Liu X, Valipour HR. Buckling of welded high-strength steel I-beams. *J Constr Steel Res* 2020;168:105938.
- [65] Fieber A, Gardner L, Macorini L. Design of structural steel members by advanced inelastic analysis with strain limits. *Eng Struct* 2019;199:109624.